Dynamical effects in X-ray spectra and the final-state rule

von Barth, Ulf; Grossmann, Günter

Published in:
Physical Review B (Condensed Matter and Materials Physics)

DOI:
10.1103/PhysRevB.25.5150

1982

PHYSICAL REVIEW B VOLUME 25, NUMBER 8 15 APRIL 1982

Dynamical effects in x-ray spectra and the final-state rule

Ulf von Barth and Günter Grossmann
Department of Theoretical Physics, University of Lund, Sweden
(Received 17 August 1981)

The dynamical theory of x-ray spectra due to Nozières and De Dominicis (ND) is evaluated here numerically for numerous model systems including cases where the core-hole potential possesses a bound state. It is shown that the resulting emission spectra obey the final-state rule rather accurately. An approximate but analytical derivation of this rule is given which provides insight into the mechanisms leading to the final-state rule. The evaluations are performed with the use of two methods, one based on an integral equation together with a separable core-hole potential and the other based on determinantal wave functions for a finite number (N) of electrons in a box. The equivalence of the two methods is demonstrated both formally and numerically. By comparing them we prove the finite-N approach to be accurate already for rather small N. We also show that a separable potential does not give rise to any spurious results but can actually be chosen to yield the same ND spectrum as a local potential. The ND theory of x-ray photoemission spectra is discussed and from calculations of the exponent function $\alpha(\omega)$ for several model systems closely corresponding to simple metals we conclude the equivalence of this theory and its asymptotic approximation as far as the extraction of asymmetry indices is concerned. Recent criticism of the major conclusions reached here and in previous work is refuted.

I. INTRODUCTION

The present paper is devoted to a discussion of current theories of x-ray spectra with regard to their capability of yielding quantitative predictions for experiments on simple metals. We will mainly be concerned with the overall shape of x-ray emission (SXE) and absorption (SXA) spectra but will also discuss the threshold singularities and the related line shape of x-ray photoemission (XPS) spectra from core levels.

Until very recently all quantitative calculations of x-ray spectra of metals were based on a one-particle approach in which the x-ray transition is viewed as occurring between a core orbital and a valence Bloch state of the perfect crystal. This simple approach is known to give an accurate description of the experimental emission spectra[1–4] and if the one-particle result is also amended with a multiplicative power-law singularity and broadened, the agreement with experiment becomes almost perfect.[5–7] Thus, the fact that there is a strong perturbing potential due to the presence of a core hole in the initial state of the emission process seems to have a very small effect on the shape of the x-ray spectrum except close to threshold. Within a one-particle approach it would have been equally justified to picture the x-ray transition as taking place between a core orbital and a valence state obtained in the one-particle potential that incorporates both the periodic solid and the screened core hole. We know now[6,9] that such a picture results in emission spectra which have very little resemblance to experimental spectra in simple metals.

In the case of x-ray absorption spectra, which probe the unoccupied valence states, there is not such a drastic difference between the two one-particle approaches—that neglecting the hole (the band case) and that accounting for the hole (the impurity case). Also, there exist no accurate calculations of x-ray absorption spectra in simple metals based on the impurity approach. Therefore, in these systems, there is not yet enough empirical evidence for preferring one approach over the other. In atoms, however, it is well known[10] that a one-particle approach will give reasonable photoabsorption cross sections only if the outgoing electron is allowed to feel the potential from the fully relaxed (screened) hole left behind.

Guided by the empirical facts presented above,[11] the present authors were led to the final-state rule[9,14] according to which accurate emission and absorption spectra of simple metals can be ob-

tained from a simple one-particle approach provided the transition matrix elements are calculated from wave functions obtained in the potential of the final state of the x-ray process, i.e., with the core hole in absorption and without the core hole in emission. The final-state rule also states that[15] even the singular behavior of the spectra near threshold can be accurately described by multiplying the one-particle result with power-law factors; one for each angular-momentum channel contributing to the spectrum. Thus, in emission, the final-state rule exactly corresponds to the commonly used procedure for interpreting experimental spectra.[5,16–21]

As mentioned above, the experimental information[1–3,6,9] leaves no doubt as to the validity of the final-state rule. However, in order to explain the rule from basic theory one clearly must go beyond the one-particle formalism and incorporate the basic dynamics of the x-ray process; namely, that a very strong perturbation due to the core hole is switched off (on) in the emission (absorption) process. The simplest possible theory which accounts for this switching is due to Nozières and DeDominicis[12] (ND). It is well known, that this theory gives a definite prediction for the shape of edge singularities in x-ray and XPS spectra. More importantly, however, the ND theory provides an answer for the overall shape of the main band of these spectra. We have previously[9,15] evaluated this theory numerically for model systems which were chosen to correspond closely to real simple metals. We then found that the resulting spectra were accurately described[22] by the final-state rule. We later evaluated the ND theory for other model systems including systems with very strong core-hole potentials. We also used different numerical methods and the results are unambiguous. As a matter of fact, to this date, no case is known for which the solution to the ND theory does not obey the final-state rule rather accurately. Since the final-state rule is in accord with experiment, so is the ND theory, which could be considered to be somewhat surprising in view of the fact that this theory does not account for the interactions between the valence electrons other than in the static screening of the core-hole potential. Dynamic screening is, e.g., not taken into account. It should, however, be remembered that the agreement between ND theory and the final-state rule or experiment, although rather good, is only approximate and there is still room for minor modifications of the spectra due to core-valence exchange and valence-valence interactions.

In retrospect the final-state rule can be considered as a restatement of basic facts. At the time it was suggested,[14] the final-state rule seemed to be rather controversial, several workers had previously either assumed or proposed what would be equivalent to an initial-state rule for emission[25–27] and also for absorption.[28] More serious, however, is the fact that the final-state rule was later implicitly challenged in a letter[29] presenting an investigation which was also based on the ND theory. In this work Swarts, Dow, and Flynn evaluated the ND theory for several model cases using a method first discussed by Friedel[30] and later used by Kotani and Toyozawa.[31] The method is based on Slater determinants for a finite number of electrons in a box. Swarts *et al.* interpreted their results for weak to moderately strong core-hole potentials as being rather well described by one-particle theory using wave functions obtained in the presence of the core hole, i.e., by an initial state rule in the case of emission. For stronger potentials they stated that the spectra could not be described by either an initial-state or a final-state rule, using the terminology introduced above. Thus, these conclusions of Swarts *et al.* are in clear contradication to our claim that the ND theory satisfies the final-state rule. Consequently, Swarts *et al.* questioned the widespread procedure implicitly based on the final-state rule and used by many workers[5,16–21] in order to interpret their experimental spectra and to extract threshold exponents. It would be a quite serious matter if these objections were justified. We show here, however, that, properly interpreted, the results of Swarts *et al.* do in fact support the final-state rule. As will be demonstrated in the present paper, this rule is indeed obeyed rather accurately by the ND theory in all cases considered.

Our earlier evaluations of the ND theory were based on the integral-equation formulation which was first introduced by Nozières and De Dominicis, and which is simplified considerably by the use of a separable potential. We will show here both formally and numerically, that this method is equivalent to the determinantal, finite-N approach used by Kotani and Toyozawa.[30,31] In fact, with only 80 s-waves in a box, the latter approach gives the same spectrum as the former within the experimental uncertainties. We will also show that realistic systems may be modeled satisfactorily by using separable core-hole potentials. For instance, a square-well potential and a separable potential give

nearly identical ND (dynamical) spectra provided the parameters of the separable potential are chosen so as to make the static initial-state spectra agree as closely as possible. In particular, the Fermi-level phase shifts and the integrated intensities should be chosen equal. In this paper we also offer further illustrations to the numerical accuracy of the final-state rule in comparison with the ND theory. We will, e.g., present results for cases where the core-hole potential is strong enough to pull a bound state out of the continuum. We will here only present results for emission because the static influence of the core hole is in this case much more drastic than in the case of absorption. For the final-state rule in absorption we refer to Ref. 15. The calculations presented in this paper were carried out using both the integral-equation formulation and the finite-N approach. In particular, we repeated several of the calculations by Swarts *et al.* to demonstrate that the resulting spectra do indeed obey the final-state rule rather accurately.

Given the accuracy of the final-state rule it would be desirable to have an explanation for the rule in simple physical terms. What we offer in this regard is only an approximate treatment within the finite-N approach, which can be solved analytically and which leads naturally to the final-state rule. This analysis also shows that the "excitonic" part of the singularity[32] is approximately multiplicative in frequency space. That part of the singularity which is due to the Anderson orthogonality catashrophe[33] and which is known to be multiplicative in time space (a convolution in frequency space) is, however, lost in this approximation.

The shape of the main line in photoemission spectra from core levels is rather accurately described in terms of the one-core-hole spectral function.[34] As mentioned above, ND theory offers a definite prediction $A_{\mathrm{ND}}(\omega)$ for this quantity. Since there is no valence-valence interaction in the ND theory, $A_{\mathrm{ND}}(\omega)$ does not have the correct satellite structure, e.g., due to plasmon production. It is, however, believed[34,35] that $A_{\mathrm{ND}}(\omega)$ provides a rather accurate description of the asymmetric main XPS line. The spectral function of the ND theory behaves asymptotically as a power-law singularity $C\omega^{\alpha-1}$ for energies ω very close to the XPS edge. This behavior with the same exponent α is generally believed[34,36] to be correct also for fully interacting electrons. This fact forms the basis for the theoretical interpretation of the experimental XPS lines which are fitted by a broadened version of the asymptotic line shape $C\omega^{\alpha-1}$.[37–39] In this way, the core-electron binding energy, the core-hole lifetime, the phonon broadening, and the asymmetry index α can be extracted from experiment.

The spectral function of ND theory, A_{ND}, obeys the sum rule $\int A_{\mathrm{ND}}(\omega)\,d\omega=1$, which expresses the fact that there must be unit probability for finding the remaining system either in the ground state or in some excited state after the XPS process. Now clearly, the asymptotic spectrum ($C\omega^{\alpha-1}$) does not obey this sum rule since the corresponding frequency integral diverges. Therefore, it is a mathematically correct but vacuous statement to say that the ND spectral function (A_{ND}) deviates from the asymptotic spectrum away from threshold ($\omega\neq 0$). Nevertheless, Dow and Flynn[40] and Bowen and Dow[41] have recently criticized the experimental procedure discussed above on precisely this ground. In this paper we will address the more relevant physical question: How large are the errors in the experimentally extracted broadenings and asymmetry indices that are introduced by using the asymptotic line shape rather than the full result of ND theory. This question we answer by computing $A_{\mathrm{ND}}(\omega)$ for model system relevant to real simple metals, applying both Lorentzian and Gaussian broadening to the result, and, finally, by trying to retrieve the input parameters (broadenings and asymmetry index α) through the fitting procedure mentioned above.[37–39] In all cases we find the errors to be smaller than the corresponding experimental uncertainties. We can thus say with confidence that ND theory is equivalent[42] to its asymptotic version in simple metals.

From this investigation we can, however, not say anything about the relevance of ND theory to real x-ray or x-ray photoemission spectra. For this we must rely on a comparison with experiment or on a deeper theoretical analysis which also accounts for the valence-valence interaction. There is, however, presently no experimental,[5,16,21,37–39] or theoretical[35] reason to expect that the results of ND theory would be substantially altered by taking this interaction into account—at least not as far as the main features of x-ray and x-ray photoemission spectra are concerned. A realistic comparison with experimental spectra also requires the inclusion of exchange effects not accounted for in ND theory. These effects can have a considerable influence on the relative intensities of, e.g., the L_2 and L_3 components of absorption spectra and may also affect the singular behavior at threshold in both emission

and absorption. We do, however, not expect any larger modification of the general shape of the spectra due to these effects.

II. THEORY OF SXE AND COMPUTATIONAL DETAILS

The determinantal approach[30,31] and the integral-equation formulation[12] represent two exact ways of solving the same problem. This equivalence will be demonstrated explicitly in this section. The integral-equation formulation was derived by Nozières and DeDominicis using the diagrammatic technique of many-body perturbation theory, which makes their work less easily accessible than the conceptually simpler determinantal approach. Following the work by Langreth,[43] we will here present an elementary but nevertheless exact derivation which assumes no familiarity with Green's-function techniques. In this section we will also give the theoretical and computational details which are needed in order to understand how the results presented in Sec. V were obtained.

We start with the golden-rule expression for the x-ray emission intensity $I(\omega)$

$$I(\omega)=\sum_f |\langle f|T|i\rangle|^2\delta(\omega+E_f-E_i) . \quad (2.1)$$

The full expression also involves a slowly varying factor $C\omega$ which has its origin in the photon degrees of freedom, but for simplicity this factor will be omitted here. It must, of course, be included before comparing to experiment. As we will present here only emission intensities, our formulas will only pertain to this case, but the case of absorption represents no additional difficulties. The initial state $|i\rangle=|N\sim\rangle$ of the emission process is assumed[8] to be the quasiground state of N valence electrons in the presence of the core hole, i.e., $c^\dagger c|N\sim\rangle=0$, where the operator c annihilates a core electron, and we write the energy of this state as $E_i=\tilde{E}_0(N)$. The possible final states $|f\rangle=c^\dagger|N-1,s\rangle$ are excited states (s) of $N-1$ valence electrons, the core orbital being occupied. The energies of these states are written as $E_f=E_s(N-1)+\epsilon_c$, where ϵ_c is the unrelaxed (e.g., Hartree-Fock) core-electron energy. The operator T, responsible for the x-ray transition, is, in the dipole approximation, given by

$$T=\sum_k p_{ck}c^\dagger a_k , \quad (2.2)$$

where $p_{ck}=\langle c|p|k\rangle$ is the one-particle dipole matrix element and where k labels a set of annihilation operators (a_k) corresponding to a complete orthonormal set $\{\psi_k(\underline{r})\}$ of one-particle valence orbitals. From the assumption above we have $cc^\dagger|N\sim\rangle=|N\sim\rangle$ giving a transition matrix element

$$\langle f|T|i\rangle=\sum_k p_{ck}\langle N-1,s|a_k|N\sim\rangle . \quad (2.3)$$

At this stage it is convenient to introduce the (unnormalized) transition-state orbital

$$\psi_b(\underline{r})=\sum_k p_{ck}^*\psi_k(\underline{r}) \quad (2.4)$$

and the corresponding annihilation operator

$$b=\sum_k p_{ck}a_k . \quad (2.5)$$

We also define the Fermi level $\epsilon_F=E_0(N)-E_0(N-1)$, the shift $\Delta=E_0(N)-\tilde{E}_0(N)$, giving the lowering of the total energy of the valence electrons upon introduction of the core-hole potential, the energy of the quasihole $E_c=\epsilon_c+\Delta$, i.e., the core-electron binding energy, and the excitation energies $\omega_s=E_s(N-1)-E_0(N-1)$ of the system of $N-1$ valence electrons. The shift Δ contains a term—$\langle N|V|N\rangle$, which is linear in the core-hole potential V, and which arises from the interaction between the core-level and the ground-state valence sea. This term is normally included in the core eigenvalue ϵ_c. The sum of the remaining terms, Δ_r, is equal to $\Delta+\langle N|V|N\rangle=\langle N|\tilde{H}|N\rangle-\langle N\sim|\tilde{H}|N\sim\rangle$ and, due to the variational principle, this sum only contains second- and higher-order terms in the potential. Therefore, Δ_r is, usually referred to as a relaxation shift.[44] Thus,

$$\Delta=\Delta_r-\langle N|V|N\rangle . \quad (2.6)$$

With these definitions, energy conservation, imposed by the δ function in Eq. (2.1), leads to the intuitively obvious result $\omega=\epsilon_F-E_c-\omega_s$, which, as $\omega_s\geq 0$, restricts the emission spectrum to lie below a threshold given by ϵ_F-E_c. Defining a shifted spectrum $J(\omega)=I(\omega-E_c)$ with the threshold at the Fermi level, $\omega=\epsilon_F$, we obtain

$$J(\omega)=\sum_s |\langle N\sim|b^\dagger|N-1,s\rangle|^2\delta(\omega+\omega_s-\epsilon_F) . \quad (2.7)$$

So far, the discussion has been quite general but in order to proceed we must take advantage of the basic assumption of ND theory, namely, that the valence electrons are scattered by the core-hole potential V in the initial state but otherwise do not interact in either initial or final state. Thus, they

are described by the noninteracting Hamiltonians

$$\tilde{H}=\sum_k \epsilon_k a_k^\dagger a_k + \sum_{k,k'} V_{kk'} a_k^\dagger a_{k'} \ . \tag{2.8}$$

and

$$H=\sum_k \epsilon_k a_k^\dagger a_k \tag{2.9}$$

in the initial state and final state, respectively. The energies ϵ_k are the usual band energies of the perfect solid. In terms of the annihilation operators $\tilde{a}_k$, corresponding to the one-particle basis set $\{\tilde{\psi}_k(\underline{r})\}$ which is obtained in the presence of the core hole and which thus diagonalizes $\tilde{H}$, these noninteracting Hamiltonians can, of course, also be written

$$\tilde{H}=\sum_k \tilde{\epsilon}_k \tilde{a}_k^\dagger \tilde{a}_k \ , \tag{2.10}$$

$$H=\sum_k \tilde{\epsilon}_k \tilde{a}_k^\dagger a_k - \sum_{k,k'} \tilde{V}_{kk'} \tilde{a}_k^\dagger \tilde{a}_{k'} \ . \tag{2.11}$$

From this basic assumption it follows that the state $|N\sim\rangle$, the ground state of $\tilde{H}$, is just a Slater determinant made up of the N lowest orbitals $\tilde{\psi}_k(\underline{r})$. Furthermore, the states $|N-1,s\rangle$ are eigenfunctions of H and can be generated from the ground-state Slater determinant $|N-1\rangle$ by creating all possible single and multiple particle-hole pair excitations. Choosing latin (greek) letters to indicate orbitals below (above) the Fermi level, we obtain the series of determinantal states: $|N-1\rangle$ [with energy $E_0(N-1)=\sum_k \epsilon_k$]; $a_\mu^\dagger a_k |N-1\rangle$ [with energy $E_0(N-1)+\epsilon_\mu-\epsilon_k$]; $a_\nu^\dagger a_\mu^\dagger a_k a_l |N-1\rangle$ [with energy $E_0(N-1)+\epsilon_\nu+\epsilon_\mu-\epsilon_k-\epsilon_l$], etc. Consequently, we find

$$J(\omega)=\langle N\sim|b^\dagger|N-1\rangle|^2\delta(\omega-\epsilon_F) + \sum_{\mu,k} |\langle N\sim|b^\dagger a_\mu^\dagger a_k|N-1\rangle|^2 \times\delta(\omega-\epsilon_F+\epsilon_\mu-\epsilon_k)+\sum_{\mu,\nu,k,l}\cdots \ . \tag{2.12}$$

Obviously, the states $b^\dagger|N-1,s\rangle$ are also Slater determinants and, therefore, all matrix elements appearing in Eq. (2.12) are simple scalar products of determinantal wave functions. Such a product is easily seen to yield the determinant of the overlap matrix of the corresponding one-particle orbitals. With a finite number (N) of valence electrons in a box, one obtains a finite levels spacing between the one-particle energies ϵ_k, but replacing the δ functions in Eq. (2.12) by normalized Gaussians with a width somewhat larger than this spacing, a continuous emission spectrum $J(\omega)$ is obtained from Eq. (2.12) by specifying the dipole matrix elements p_{ck} and the one-particle overlap integrals $\langle\tilde{\psi}_k|\psi_{k'}\rangle$. The evaluation of the first term in Eq. (2.12) requires of the order of N^3 elementary arithmetric operations. As a by-product of this evaluation one obtains the so-called minors of the determinant $\langle N\sim|b^\dagger|N-1\rangle$, from which each term (μ,k) in the sum of the second term is obtainable by ca. N operations. Summing over a set of orbitals ψ_μ also chosen to be of order N, the computation of the contribution from the single-pair excitations, i.e., the second line of Eq. (2.12), is again an N^3-operation. The double-pair excitations, i.e., the third line in Eq. (2.12), however, present a problem of order N^4, and higher excitations becomes exceedingly more time consuming. With an increasing number (N) of electrons, i.e., with a decreasing level spacing, these higher excitations contribute a larger and larger fraction of the total emission intensity, eventually rendering the determinantial approach intractable. Fortunately, it is possible to find an N (ca. 100) such that almost all intensity is given by single-pair excitations and such that the shape of the resulting spectrum is very close to the spectrum obtained in an infinite system ($N\to\infty$). This is a somewhat unexpected result for which we have no simple physical explanation, but which nevertheless makes the determinantal approach a very convenient way to evaluate the ND theory. All *emission* results from this approach presented in the present work were obtained by including only single-pair excitations, i.e., by truncating the expansion on the right-hand side of Eq. (2.12) after the second term. In Fig. 1 we compare the result of the determinantal approach using 80 s electrons in a box with the corresponding result for the infinite system obtained from the integral equation [Eq. (2.29)] to be derived below, and the agreement is indeed striking.

The convergence of the determinantal approach with respect to N towards the limit of a very large system can also be studied from the sum rule obeyed by the integrated emission intensity. This quantity is easily obtained from Eq. (2.7) by using the completeness of the states $|N-1,s\rangle$

$$\int_{-\infty}^{\epsilon_F} J(\omega)\,d\omega=\langle N\sim|b^\dagger b|N\sim\rangle \ . \tag{2.13}$$

By expressing the operator b in terms of the basis set $(\tilde{\psi}_k)$ obtained in the presence of the core hole [cf. Eq. (2.5)], the right-hand side of Eq. (2.13) becomes $\sum_{k,k'}\langle N\sim|\tilde{a}_k^\dagger\tilde{a}_{k'}|N\sim\rangle\tilde{p}_{ck}^*\tilde{p}_{ck'}$, and consequently, from the definition of the quasiground

state $|N\sim\rangle$,

$$\int_{-\infty}^{\epsilon_F} J(\omega)\,d\omega=\sum_{k}^{\text{occ}}|\tilde{p}_{ck}|^2\,, \tag{2.14}$$

where "occ" indicates that the sum extends over the N lowest orbitals $\tilde{\psi}_k$. At this stage it is convenient to introduce two other concepts central to our discussion—the static initial-state spectrum, $J_i(\omega)$, and the static final-state spectrum, $J_f(\omega)$. These are defined as the shifted spectra obtained within simple one-particle theory with core-valence dipole matrix elements computed from valence orbitals obtained in the presence of the core hole and in the absence of the hole, respectively. Thus

$$J_i(\omega)=\sum_{k}^{\text{occ}}|\tilde{p}_{ck}|^2\delta(\omega-\tilde{\epsilon}_k)\,, \tag{2.15}$$

$$J_f(\omega)=\sum_{k}^{\text{occ}}|p_{ck}|^2\delta(\omega-\epsilon_k)\,, \tag{2.16}$$

and the sum rule [Eq. (2.14)] then shows that the integrated intensity of the dynamical spectrum $J(\omega)$ is equal to that of the static initial-state spectrum (see also Ref. 13). When only single-pair excitations are included in the dynamical spectrum, its integrated intensity does not exhaust the sum rule and the error increases not only rapidly with N, but also with the strength of the core-hole potential. We have, however, found numerically that, for N ca. 80, no more than 4% of the total intensity is contributed by double pair and higher excitations, even for very strong potentials that almost result in a bound state.

Having discussed the determinantal approach, we will now concentrate on the equivalent approach originally presented by Nozières and DeDominicis.[12] This method leads to an integral equation whose solution in turn determines the x-ray spectrum. The solution is, however, rather difficult to obtain for ordinary local core-hole potentials, a disadvantage not encountered in the determinantal approach. One of the clear advantages of the integral-equation formulation lies in the fact that the equation can be solved asymptotically to yield the singular behavior of the spectra close to threshold.[12] The main reason why we have chosen to base most of our work on this approach is, however, that it can rather easily be generalized to include the interaction between the electrons, thus eventually enabling us to go beyond ND theory. Such a generalization is very difficult to attain in the determinantal approach.

The starting expression is the same as for the determinantal approach, Eq. (2.7). The first step is to convert the δ function into an integral in time-space giving

$$J(\omega)=\frac{1}{\pi}\,\mathrm{Re}\sum_{s}\int_{-\infty}^{0}dt\,e^{it(\omega+\omega_s-\epsilon_F)}\times\langle N\sim|b^\dagger|N-1,s\rangle\times\langle N-1,s|b|N\sim\rangle\,. \tag{2.17}$$

Then, from the definition of ω_s [$\omega_s=E_s(N-1)-E_0(N-1)=E_s(N-1)-\tilde{E}_0(N)+\tilde{E}_0(N)-E_0(N)+E_0(N)-E_0(N-1)=E_s(N-1)-\tilde{E}_0(N)-\Delta+\epsilon_F$] and from the completeness of the eigenstates $|N-1,s\rangle$ of H we obtain

$$J(\omega)=\frac{1}{\pi}\mathrm{Re}\int_{-\infty}^{0}dt\,e^{it(\omega-\Delta)}\langle N\sim|b^\dagger e^{iH}be^{-it\tilde{H}}|N\sim\rangle\,. \tag{2.18}$$

Expanding b, for later convenience in the basis that diagonalizes $\tilde{H}$, the spectrum is finally given by

$$J(\omega)=\frac{1}{\pi}\,\mathrm{Re}\sum_{k,k'}\tilde{p}_{ck}\tilde{p}^*_{ck'}\int_{-\infty}^{0}dt\,e^{it(\omega-\Delta)}\tilde{F}_{kk'}(t)\,, \tag{2.19}$$

provided we know the correlation function

$$\tilde{F}_{kk'}(t)=\langle N\sim|a^\dagger_{k'}e^{iHt}\tilde{a}_k e^{-i\tilde{H}t}|N\sim\rangle\,. \tag{2.20}$$

In Appendix A we show that $\tilde{F}_{kk'}(t)$ is a product of two quantities $\tilde{G}_{kk'}(t,t)$ and $\tilde{g}(t)$,

$$\tilde{F}_{kk'}(t)=-i\tilde{g}(t)\tilde{G}_{kk'}(t;t) \tag{2.21}$$

and that $\tilde{G}_{kk'}(\tau,t)$ can be obtained from the integral equation

$$\tilde{G}_{kk'}(\tau;t)=\tilde{G}^0_k(\tau)\delta_{kk'}+\sum_{q}\int_0^t\tilde{G}^0_k(\tau-\tau')\times\tilde{V}_{kq}G_{qk'}(\tau';t)\,d\tau'\,, \tag{2.22}$$

involving a free-particle Green's function

$$\tilde{G}^0_k(\tau)=-ie^{-i\tilde{\epsilon}_k\tau}[(1-\tilde{n}_k)\Theta(\tau)-\tilde{n}_k\Theta(-\tau)]\,. \tag{2.23}$$

Here, $\Theta(\tau)$ is the usual Heaviside step function and the Fermi factor $\tilde{n}_k$ is one or zero depending on whether the state k is occupied or not. The integral equation completely determines $\tilde{G}_{kk'}(\tau,t)$ in

the interval $t<\tau<0$ and in Appendix A we also show that $\tilde{g}(t)$ can be obtained from $\tilde{G}_{kk'}$ according to

$$\tilde{g}(t)=\exp\left[\sum_{k,k'}\int_t^0 \tilde{V}_{k'k}\tilde{G}_{kk'}(0;\tau)\,d\tau\right] . \tag{2.24}$$

Thus, in order to compute the emission spectrum we must first solve the integral equation (2.22) for a given core-hole potential, then obtain $\tilde{g}(t)$ from Eq. (2.24) and $\tilde{F}_{kk'}(t)$ from Eq. (2.21), and finally we must evaluate the Fourier transform and perform the sums prescribed by Eq. (2.19). The principal difficulty of this procedure lies in obtaining a solution to Eq. (2.22). For real solids, the label k is three-dimensional and we have an integral equation in four variables. Assuming a local spherical core-hole potential the equation can in many cases be reduced to a set of coupled integral equations in two variables but the solution to this simpler problem still requires a considerable effect. However, using a separable potential of the form

$$\tilde{V}_{kk'}=V_0\tilde{p}^*_{ck}\tilde{p}_{ck'} \tag{2.25}$$

reduces the calculation of the spectrum to a truly one-dimensional problem in time-space. In writing the core-hole potential as in Eq. (2.25) we have actually introduced two approximations: (i) the potential is separable and (ii) the k dependence is governed by that of the dipole matrix element. It might appear as if the second approximation imposes too severe a restriction on the potential by leaving only one free parameter, V_0, in order to model a realistic core-hole potential. It is, however, seen from Eq. (2.20) that $\tilde{F}_{kk'}(t)$ is nonzero only if both k and k' label occupied states and, therefore, by virtue of Eq. (2.19), we need the dipole matrix element $\tilde{p}_{ck}$ only below the Fermi level in order to obtain the spectrum. Consequently, we are free to chose $\tilde{p}_{ck}$ above the Fermi level at will and, in the present paper, we will show that this additional freedom sufficies to allow us to model any local potential pertinent to a simple metal by means of the ansatz (2.25). We will use the determinantal approach, in which a local potential is no more difficult to treat than a separable potential, to show that, given a local potential we can find a separable model potential [Eq. (2.25)], which is equivalent to the former in the sense that both potentials give rise to almost the same dynamical spectrum.

We now demonstrate that, with the ansatz (2.25), our problem becomes essentially one-dimensional and comparatively simple. We define the auxiliary quantity

$$\tilde{G}(\tau,t)=\sum_{k,k'}\tilde{p}_{ck}\tilde{G}_{kk'}(\tau,t)\tilde{p}^*_{ck'} \tag{2.26}$$

in terms of which the spectrum is given by [Eqs. (2.19) and (2.21)]

$$J(\omega)=\frac{1}{\pi}\mathrm{Im}\int_{-\infty}^0 e^{it(\omega-\Delta)}\tilde{g}(t)\tilde{G}(t;t)\,dt . \tag{2.27}$$

Similarly we define the Green's function

$$\tilde{G}^0(\tau)=\sum_k\tilde{p}_{ck}\tilde{G}^0_k(\tau)\tilde{p}^*_{ck} . \tag{2.28}$$

If we now multiply the integral equation (2.22) from the left by $\tilde{p}_{ck}$ and from the right by $\tilde{p}^*_{ck'}$ and sum over k and k', these definitions and the ansatz (2.25) lead to the one-dimensional integral equation

$$\tilde{G}(\tau;t)=\tilde{G}^0(\tau)+V_0\int_0^t\tilde{G}^0(\tau-\tau')\times\tilde{G}(\tau';t)\,d\tau' , \tag{2.29}$$

and Eq. (2.24) becomes

$$\tilde{g}(t)=\exp\left[V_0\int_t^0\tilde{G}(0;\tau)\,dt\right] . \tag{2.30}$$

In terms of the density of states $\mathscr{D}(\epsilon)$, we also define the transition density of states (TDOS) obtained in the presence of the core-hole potential, $\tilde{A}(\omega)$, and the TDOS for the ground-state solid with a filled core level, $A(\omega)$, by

$$\tilde{A}(\omega)=[\mathscr{D}(\epsilon_k)\,|\,\tilde{p}_{ck}\,|^2]_{\epsilon_k=\omega} , \tag{2.31}$$

$$A(\omega)=[\mathscr{D}(\epsilon_k)\,|\,p_{ck}\,|^2]_{\epsilon_k=\omega} , \tag{2.32}$$

where p_{ck} now is an averaged matrix element depending only on energy. Then the static initial- and final-state spectra defined by Eqs. (2.15) and (2.16) are given by the occupied part of the TDOS obtained in the presence and in the absence of the core hole, respectively.

$$J_i(\omega)=\tilde{A}(\omega)\Theta(\epsilon_F-\omega) , \tag{2.33}$$

$$J_f(\omega)=A(\omega)\Theta(\epsilon_F-\omega) . \tag{2.34}$$

With these definitions we find that the Green's function $\tilde{G}^0(\tau)$ of Eq. (2.28) is completely specified by the TDOS of the initial state with the core hole,

$$\tilde{G}^0(\tau)=-i\Theta(\tau)\int_{\epsilon_F}^{\infty}\tilde{A}(\epsilon)e^{-i\epsilon\tau}d\epsilon +i\Theta(-\tau)\int_{-\infty}^{\epsilon_F}\tilde{A}(\epsilon)e^{-i\epsilon\tau}d\epsilon . \tag{2.35}$$

With the ansatz (2.25), $\tilde{A}(\omega)$ can, as shown in Appendix B, be evaluated analytically to yield the result

$$\tilde{A}(\epsilon)=A(\epsilon)\left[\left[1-V_0\int\frac{A(\epsilon')\,d\epsilon'}{\epsilon-\epsilon'}\right]^2+V_0^2\pi^2A^2(\epsilon)\right]^{-1} \quad (2.36)$$

in terms of the TDOS $A(\omega)$ of the final state, i.e., the TDOS of the perfect solid. In Appendix B we also show that the Fermi-level phase shift δ_F of the separable potential [Eq. (2.25)] is given by

$$\sin\delta_F=-V_0\pi[A(\epsilon_F)\tilde{A}(\epsilon_F)]^{1/2}\,. \quad (2.37)$$

From Eqs. (2.36), (2.35), (2.29), (2.30), and (2.27) we see that the dynamical emission spectrum is completely determined by the TDOS $A(\omega)$ of the final state and the potential parameter V_0. All results from the integral-equation approach presented in this work were obtained from these equations.

We will now describe the procedure used in our practical applications. In order to obtain the dynamical emission spectrum for a real solid, i.e., the spectrum predicted by ND theory, we first compute the static final-state spectrum for the solid, i.e., the spectrum obtained from one-particle theory in which the valence Bloch functions are used to calculate the transition matrix elements. Due to dipole selection rules, this spectrum has in general two angular-momentum components. For instance, in the case of a core hole of p character, there is an s and a d contribution to the spectrum. We will consider these contributions separately, one at a time. Such a procedure is based on the assumption that the full ND integral equation (2.22) is to a good approximation equivalent to a set of decoupled integral equations, one for each angular-momentum channel. It is not difficult to show that this really is the case in a simple metal with cubic symmetry, assuming a spherical core-hole potential and neglecting $l=4$ and higher angular-momentum components of the Green's function in the central cell. An ansatz of the form given by Eq. (2.25) can then be made for each angular-momentum channel. For each channel we identify $A(\omega)$ below the Fermi level, i.e., the static final-state spectrum, with the transition density of states of the real system. From self-consistent impurity calculations for the real system with a core hole on one site, we next obtain the screened core-hole potential, the corresponding Fermi-level phase shifts, and the angular-momentum decomposed transition density of states in the presence of the core hole.[6] For each channel we then determine V_0 and $A(\omega)$ *above* the Fermi level by the requirement that the phase shift given by Eq. (2.37) be the same as the true Fermi-level phase shift and that $\tilde{A}(\omega)$ from Eq. (2.36) be an optimal fit to the occupied part of the TDOS of the real system in the presence of the core hole. Due to the severe restrictions imposed by our separable ansatz [Eq. (2.25)], the fitted TDOS, i.e., the fitted initial-state spectrum, may deviate considerably from the full result. A typical example is provided in Fig. 2, where the full result is represented by the TDOS of a free-electron gas in the presence of a spherical square-well potential. Owing to the sum rule given by Eq. (2.14), the weight of the dynamical spectrum, i.e., the integrated intensity below the Fermi level, is given by the weight of the static initial-state spectrum and, therefore, it is essential to ensure that at any rate the weight of the fitted spectrum $\tilde{A}(\omega)$ be equal to that of the static initial-state spectrum of the real solid.

Having obtained $A(\omega)$ and V_0 in this way, we compute the Green's function $\tilde{G}^0(\tau)$ from Eq. (2.35) and solve the integral equation (2.29). For moderately large times, this equation can be solved by straightforward iteration, but for large t and strong potentials V_0, the iteration converges rather slowly. Therefore, in practice, we used a technique based on Padé approximants.[45] A few further parameters enter into the numerical procedures. The density of states of a particular angular momentum decays rather slowly for large energies. The dipole matrix elements, however, tend to zero rather rapidly at larger energies and, consequently, so does $A(\omega)$ [Eq. (2.32)]. Since our procedure allows us to choose $A(\omega)$ rather freely above the Fermi level, we have decided to make it vanish above some high energy ϵ_M, usually chosen to be ca. $4\epsilon_F$. The inverse of the total energy range of $A(\omega)$ [and of $\tilde{A}(\omega)$, Eq. (2.36)] will set the time scale for fine structure in the Green's function $\tilde{G}^0(\tau)$. Thus the time step Δt of Simpson's rule that we used to evaluate the integral in Eq. (2.29) had to be chosen to be $\sim 1/(4\epsilon_M)$. Having solved the integral equation up to a maximal time $|t_M|$, we have to perform a Fourier transform [Eq. (2.27)] to obtain the spectrum. As merely cutting this integral at t_M introduces artifical oscillations, one can choose to obtain a broadened spectrum by including a factor $\exp(-\alpha|t|)$ (Lorentzian) or $\exp(-\beta t^2)$ (Gaussian) in the integrand, with parameters α or β chosen such that the integrand essentially vanishes beyond $|t_M|$. But in order to obtain a better resolution and an accurate descrip-

tion of the sharp singular feature at the Fermi edge, we apply a fitting procedure that allows us to do the Fourier integral analytically for large times ($t \to -\infty$). For large times the two main quantities $\tilde{G}(0,t)$ and $\tilde{G}(t,t)$, which according to Eqs. (2.27) and (2.30) determine the SXE spectrum, are fitted to the analytical expressions

$$V_0\tilde{G}(0;t)=\frac{\delta_0^2}{\pi^2}\frac{1}{t}-iD_0+C_0t^{-\beta}e^{i(\Omega_0 t+\phi_0)}, \quad (2.38)$$

$$e^{i\epsilon_F t}\tilde{G}(t;t)=De^{i\delta_1}|t|^{[2(\delta_2/\pi)-1]}+Ct^{-\gamma}e^{i(\Omega t+\phi)}. \quad (2.39)$$

The real fitting parameters C_0, C, D_0, D, Ω_0, Ω, ϕ_0, ϕ, β, γ, δ_0, δ_1, and δ_2 are chosen so as to yield the least-square's deviation between these expressions and the corresponding quantities obtained from the integral equation. The fitting is done over time intervals of the form $(\sim\frac{2}{3}t_M, t_M)$ and repeated for successively larger $|t_M|$ until the fitting parameters remain almost unchanged. In this way we obtain a nearly exact solution to the integral equation valid for all negative times. The analytical expressions were certainly not chosen *ad hoc*. Clearly, the constant term in Eq. (2.38) determines the position of the x-ray threshold [Eqs. (2.27) and (2.30)] and the fitting parmeter D_0 should converge to Δ in order to fix the threshold at the Fermi level ϵ_F. The first term of Eq. (2.38) contributes a factor $(\epsilon_F-\omega)^{(\delta_2/\pi)^2}$ to the singular-threshold behavior. Provided the fitting parameter δ_0 equals δ_F i.e., the Fermi-level phase shift of the core-hole potential, this is the correct suppression of the x-ray edge due to the Anderson "orthogonality catastrophy."[33] Similarly, the first term of Eq. (2.39) yields, close to threshold, a factor $(\epsilon_F-\omega)^{-2(\delta_2/\pi)}$, which is the correct excitonic enhancement of the edge,[32] provided the parameter δ_2 also equals δ_F. Furthermore, it follows from the asymptotic version of ND theory[12] that we should also obtain $\delta_1=\delta_F$. The last terms in Eqs. (2.38) and (2.39) are meant to describe the oscillations in time produced by the nonanalytic behavior of the TDOS at the bottom of the band.[46] It is indicative of the internal consistency of the fitting procedure and of the overall accuracy of our numerical procedure that the parameters obtained in an unrestricted fit did, within a few percent, fulfill the requirements discussed above. This result can also be viewed as a numerical verification of the asymptotic expressions derived by ND.[12]

As demonstrated above, the integral equation approach is made quite tractable by means of the ansatz (2.25) but in order to show that this approach gives accurate ND spectra we must compare the results with those obtained from a more realistic potential. For this purpose we have assumed that a realistic core-hole potential can be modeled by a local energy-independent potential. At least away from the Fermi level this might be a questionable approximation since the true interaction between a quasiparticle and the core hole, i.e., the difference in the self-energies with and without the hole, is both nonlocal and energy dependent. However, we do not expect this approximation to be serious[47] and in any case it is consistent with ND theory which also neglects the valence-valence interactions. Furthermore, we have decided to use a spherical square-well potential as a typical example of a local core-hole potential in a simple metal. We believe this to be a reasonable choice for s and p electrons in view of the fact that actual core-hole potentials are small and monotonically increasing functions of the distance to the nucleus.[6] Thus, in this paper we will show that the emission spectrum resulting from switching off a square-well potential in an otherwise free-electron gas can be accurately modeled by replacing the square-well potential with the separable ansatz (2.25). We note that a square-well potential makes the determinantal method rather trivial to carry out since the wave functions confined to a large sphere of radius S can be obtained analytically both with $\{\tilde{\psi}_k\}$ and without $\{\psi_k\}$ the potential at the center. The required overlap integrals $\int^S \tilde{\psi}_k^*(\underline{r})\psi_{k'}(\underline{r})\,d^3r$ can also be obtained analytically but we will not give these trivial formulas here. The dipole matrix elements p_{ck} can be chosen at will, e.g., for the s part of the spectrum they can be simulated by $\int e^{-r/r_c}\times\psi_k(\underline{r})\,d^3r$ with a suitable core radius r_c or they can be taken as the wave function at the origin $[\psi_k(0)]$ as is done by Swarts *et al.*[29] The former choice makes it easy to simulate a one-particle emission spectrum of a real simple metal but the latter is somewhat unphysical. It results in a spectrum with a square-root energy dependence at all energies and the matrix elements p_{ck} do not tend to zero as they should. Furthermore, the choice made by Swarts *et al.* overestimates the ratio between the integrated intensities of the static initial- and final-state spectra. In a monovalent metal this ratio is approximately two, reflecting the approximate proportionality between the spectra and the local-state densities and the fact that the core hole

is screened by exactly one additional valence electron in the central cell.

III. THEORY OF XPS

In this section we will merely summarize those details of the theory of x-ray photoemission[48] that would enable the reader to repeat the calculations leading to the results presented in Sec. V. In the so-called sudden approximation, which will be used here and which leads to a description of XPS in terms of the one-core-hole Green's function, this theory is actually a simpler version of the theory of x-ray emission presented in Sec. II. Therefore, we can rely heavily on the results obtained there. The starting point is the same, the golden rule

$$I(\omega)=\sum_f |\langle f|T|i\rangle|^2\delta(\nu+E_i-E_f) \times\delta(\omega+\epsilon_F-\epsilon_k)\ , \tag{3.1}$$

where we have inserted an extra δ function to account for the fact that the photoemitted electrons are usually analyzed according to their energy relative to the Fermi level, $\epsilon_k-\epsilon_F$. The energy ν of the exciting photon is assumed to be very large, resulting in a high kinetic energy ($\sim\epsilon_k$) of the photoemitted electron which then can be treated approximately as a free electron. The initial and final states of the XPS experiment differ from those of SXE. The initial state $|i\rangle$ is the ground state of N valence electrons and an occupied core orbital, $c^\dagger|N\rangle$, and its energy is $E_0(N)+\epsilon_c$, in the notation of Sec. II. In the sudden approximation the final state is written as $a_k^\dagger|N,s\sim\rangle$, representing an outgoing bare electron in a state k that does not interact with the excited state s of the N valence electrons which are left in the presence of a core hole. The final-state energy is $\tilde{E}_s(N)+\epsilon_k$. The part of the transition operator T which couples the initial state to the chosen final states is now the Hermitian conjugate to Eq. (22)

$$T=\sum_k p_{ck}^* a_k^\dagger c\ . \tag{3.2}$$

The matrix element $\langle f|T|i\rangle$ becomes $\sum_{k'}p_{ck'}^*\times\langle N,s\sim|a_k a^\dagger_{k'}cc^\dagger|N\rangle$. By definition $cc^\dagger|N\rangle=|N\rangle$, and we can safely assume that there is a negligible content of one-particle states with the very high energy ϵ_k in the ground state $|N\rangle$. Thus

$$\langle f|T|i\rangle=p_{ck}^*\langle N,s\sim|N\rangle\ , \tag{3.3}$$

and by rearranging the eneriges in the δ functions and using our definitions from Sec. II $E_0(N)-\tilde{E}_s(N)+\epsilon_c-\epsilon_k=\Delta_r-\tilde{\omega}_s+\epsilon_c-\omega-\epsilon_F=E_c-\epsilon_F-\tilde{\omega}_s-\omega$, we obtain

$$I(\omega)=\sum_k\sum_s |p_{ck}|^2|\langle N,s\sim|N\rangle|^2 \times\delta(\nu+E_c-\epsilon_F-\tilde{\omega}_s-\omega) \times\delta(\omega+\epsilon_F-\epsilon_k)\ . \tag{3.4}$$

Introducing the density of states $\mathcal{D}(\epsilon)$ to convert the sum over the label k to an integral over energies, we have

$$I(\omega)=\mathcal{D}(\omega+\epsilon_F)|p_{ck}|^2_{\epsilon_k=\omega+\epsilon_F} \times\sum_s|\langle N,s\sim|N\rangle|^2 \times\delta(\omega+\tilde{\omega}_s-\nu-E_c+\epsilon_F)\ , \tag{3.5}$$

which shows that the threshold of the XPS spectrum is again determined by the core-electron binding energy relative to the Fermi energy ϵ_F-E_c as was the threshold of the SXE spectrum. At high energies ω, the TDOS factor in front of the sum over excited states s varies slowly with energy and can be considered as a constant over the width of the XPS line. Since absolute intensities are not measured, this constant can be omitted together with other slowly varying factors that actually should have appeared in front of the golden-rule expression. Being primarily interested in the shape of the XPS line and not in its position, we define our shifted and unnormalized spectrum $A_c(\omega)$ to be

$$A_c(\omega)=\sum_s|\langle N|N,s\sim\rangle|^2\delta(\omega+\tilde{\omega}_s)\ . \tag{3.6}$$

Obviously, the threshold has been shifted from $\omega=\nu+E_c-\epsilon_F$ to $\omega=0$, i.e., $A_c(\omega)=0$ for $\omega\geq 0$. Owing to the completeness of the states $|N,s\sim\rangle$,[49] the unnormalized spectrum fulfills the convenient sum rule

$$\int_{-\infty}^0 A_c(\omega)\,d\omega=1\ . \tag{3.7}$$

Comparing the Eqs. (2.7) and (3.6) we see that XPS from a theoretical point of view, is indeed a simpler version of SXE. The determinantal technique for XPS is almost identical to that of SXE. The determinants $b^\dagger|N-1,s\rangle$ in SXE are replaced by determinants $|N,s\sim\rangle$ in XPS, the single-pair and higher-order excitations, however, are now to be described in the core-hole basis $\{\tilde{a}_k,\tilde{\psi}_k(\underline{r})\}$ which, for absorption, again corresponds to the final state of the system. The excitation energies should also be obtained in the pres-

ence of the core hole, although the distinction between core-hole ($\tilde{\epsilon}_k$) and no-core-hole (ϵ_k) eigenvalues becomes irrelevant already at rather small N. Thus

$$A_c(\omega)= |\langle N|N\sim\rangle|^2\delta(\omega) + \sum_{\mu,k} |\langle N|\tilde{a}_\mu^\dagger \tilde{a}_k|N\sim\rangle|^2\delta(\omega+\tilde{\epsilon}_\mu-\tilde{\epsilon}_k) + \sum_{\mu,\nu,k,l} |\langle N|\tilde{a}_\mu^\dagger\tilde{a}_\nu^\dagger\tilde{a}_k\tilde{a}_l|N\sim\rangle|^2 \times\delta(\omega+\tilde{\epsilon}_\mu+\tilde{\epsilon}_\nu-\tilde{\epsilon}_k-\tilde{\epsilon}_l)+\cdots . \tag{3.8}$$

For systems, with of the order of 100 s waves in a box we have found numerically that the contributions from double pair excitations [third line of Eq. (3.8)] are very small and that higher-order excitations can be neglected. Only if a very high accuracy is required in connection with strong core-hole potentials may double excitations be of some importance. This is demonstrated in Table I which, for two spherical square-well potentials of different strengths, shows how well the spectrum fulfills the sum rule (3.7) when no excitations, single excitations, and also double excitations are included.

The equivalent integral-equation approach to the XPS spectrum is obtained in a way similar to that leading to the SXE spectrum, namely, by expressing the δ function in Eq. (3.6) as an integral over time t giving

$$A_c(\omega)=\frac{1}{\pi}\mathrm{Re}\int_0^\infty dt\, e^{i\omega t} \times\sum_s e^{i\tilde{\omega}_s t}\langle N|N,s\sim\rangle\langle N,s\sim|N\rangle . \tag{3.9}$$

From the definition in Sec. II we have $\tilde{\omega}_s=\tilde{E}_s(N)-\tilde{E}_0(N)=\Delta+\tilde{E}_s(N)-E_0(N)$ and using the completeness of the states $|N,s\sim\rangle$ we have

$$A_c(\omega)=\frac{1}{\pi}\mathrm{Re}\int_0^\infty dt\, e^{it(\omega+\Delta)}g(t) , \tag{3.10}$$

where we defined the function $g(t)$ by

$$g(t)=\langle N|e^{i\tilde{H}t}e^{-iHt}|N\rangle . \tag{3.11}$$

This function is quite analogous to the function $\tilde{g}(t)$ defined for the case of x-ray emission in Appendix A [Eq. (A8)], and $g(t)$ has to be obtained from an integral equation similar to that determining $\tilde{g}(t)$ [Eqs. (2.22) and (2.24)]. The derivation of this new equation differs only in minor details from the derivation of, e.g., Eq. (2.22) and we will here give only the final results for the case of the separable potential defined in Eq. (2.25).[50] We obtain the integral equation

$$G(\tau;t)=G^0(\tau)+V_0\int_0^t G^0(\tau-\tau')G(\tau';t)\,d\tau' , \tag{3.12}$$

where $G^0(\tau)$ is the noninteracting Green's function in the absence of the core hole given by

$$G^0(\tau)=-i\Theta(\tau)\int_{\epsilon_F}^\infty A(\epsilon)e^{-i\epsilon\tau}d\epsilon +i\Theta(-\tau)\int_{-\infty}^{\epsilon_F}A(\epsilon)e^{-i\epsilon\tau}d\epsilon , \tag{3.13}$$

in terms of $A(\epsilon)$, the transition density of states in the absence of the core hole. This integral equation uniquely determines the quantity $G(\tau;t)$ in the interval $0\le\tau\le t$ and the function $g(t)$ is then given by

$$g(t)=\exp\left[+itV_0\int A(\epsilon)\,d\epsilon - V_0\int_0^t G^*(0;\tau)\,d\tau\right] . \tag{3.14}$$

Thus, in order to compute an XPS spectrum of a

TABLE I. The integral $S=\int_{-4\epsilon_F}^0 A_c(\omega)\,d\omega$ over the spectral function $A_c(\omega)$ from the finite-N approach is here shown as a function of N for two different square wells when no excitations (S_0), single-pair excitations (S_1), and double-pair excitations (S_2) are included in the sum over final states in Eq. (3.8).

	$\delta_F=0.20\pi$			$\delta_F=0.41\pi$		
N	S_0	S_1	S_2	S_0	S_1	S_2
40	0.835	0.995	0.997	0.457	0.971	0.994
80	0.814	0.994	0.997	0.406	0.955	0.994
150	0.794	0.992	0.997	0.365	0.937	0.993

real solid—or for that matter an absorption spectrum (see below)—we identify $\tilde{A}(\epsilon)$ above the Fermi level with the one-particle transition density of states of the solid in the presence of the core hole. We then obtain $A(\epsilon)$ from the inverse of Eq. (2.36) where we have chosen V_0 such that the Fermi-level phase shift from Eq. (2.37) is equal to that of the full core-hole potential and where $\tilde{A}(\epsilon)$ below the Fermi level has been chosen to yield a good fit above the Fermi level between $A(\epsilon)$ and the one-particle transition density of states of the ground-state solid. Finally we calculate the Green's function $G^0(\tau)$ from Eq. (3.13), solve the integral equation (3.12), and compute the function $g(t)$ from Eq. (3.14) and the XPS spectrum from Eq. (3.10). If there are several important angular momentum channels the resulting spectra of each channel must be convoluted to form the total XPS spectrum. In simple metals it is essential to include both the s and the p channels, while the d channel can be neglected.[15]

The XPS experiment can be thought of as an absorption experiment carried out at high energies and it is thus not surprising that the SXA spectrum $J_{\mathrm{SXA}}(\omega)$ can also be obtained from the procedure described above. Choosing the threshold at $\omega=\epsilon_F$ it is given by [cf. Eq. (2.27)]

$$J_{\mathrm{SXA}}(\omega)=-\frac{1}{\pi}\,\mathrm{Im}\int_0^\infty dt\, e^{it(\omega-\Delta)}g^*(t)G(t;t)\ . \tag{3.15}$$

This equation has been used in Ref. 15 to demonstrate the accuracy of the final-state rule for absorption in several model systems. In the present paper we will, however, not present any absorption results.

In the free-electron approximation the XPS spectrum is simply a δ function and in ND theory it becomes a rather narrow sharp peak which asymptotically approaches a power-law singularity at the edge. For very strong core-hole potentials there can be structure due to strong shake-up processes at energies $\sim\epsilon_F$ below the edge but there will be no satellite structure due to plasmons since there is no valence-valence interaction in the ND model. For simple metals, however, most of the total intensity is concentrated close to the edge and consequently, it is quite difficult, by just looking at $A_c(\omega)$, to determine the energy range in which the actual ND spectrum approximately follows a power law. Therefore, we have here decided to show our results for $A_c(\omega)$ in a more illustrative way,[51] in which the deviation from the asymptotic line shape becomes more apparent. To this end we define the exponent function $\alpha(t)$ according to

$$\alpha(t)=\begin{cases}\dfrac{iV_0}{2\pi}G^*(0;t)+\dfrac{\beta}{2\pi}, & t\geq 0\\ \alpha^*(-t), & t\leq 0,\end{cases} \tag{3.16}$$

where β is short for $\Delta+V_0\int A(\epsilon)\,d\epsilon$. From the Eqs. (3.10) and (3.14) we see that the spectral function $A_c(\omega)$ can be written as

$$A_c(\omega)=\frac{1}{2\pi}\int dt\, e^{i\omega t}\exp\left[2\pi i\int_0^t\alpha(\tau)\,d\tau\right]\ . \tag{3.17}$$

In analogy with Eq. (2.38) it can be shown[12] that the function $V_0G(0;t)$, for large t, behaves asymptotically as

$$V_0G(0;t)=-i\beta+\frac{\alpha}{t}\ , \tag{3.18}$$

where the asymmetry index α of one angular momentum and spin channel is given by

$$\alpha=\delta_F^2/\pi^2 \tag{3.19}$$

in terms of the Fermi-level phase shift δ_F of that channel. Thus, for large t we have asymptotically $\alpha(t)=i\alpha/(2\pi t)$. At energies close to the edge, i.e., for small frequencies in $A_c(\omega)$, the dominant contribution to the Fourier integral in Eq. (3.17) comes from large t and by introducing a cut-off T in the integration over τ and replacing $\alpha(t)$ with its asymptotic form, both integrals in Eq. (3.17) can actually be carried out analytically, and to logarithmic accuracy we obtain

$$A_c(\omega)=C\,|\,\omega\,|^{\alpha-1}\ . \tag{3.20}$$

This is the asymptotic line shape derived by Nozières and DeDominicis but the constant C depends on details of the potential in a more complicated way than simply via the Fermi-level phase shifts and cannot be obtained from the asymptotic arguments presented above. Obviously, the exponent function $\alpha(t)$ decays fast enough to be Fourier transformed and we have

$$\alpha(\omega)=\frac{1}{\pi}\,\mathrm{Im}\int_0^\infty dt\, e^{-i\omega t}[V_0G(0;t)+i\beta]\ . \tag{3.21}$$

If we multiply Eq. (3.17) by ω, integrate by parts, and introduce the inverse of this Fourier transform, we obtain the relation $\omega A_c(\omega)=-\int d\omega'\,\alpha(\omega')A_c(\omega-\omega')$. Since the spectral function $A_c(\omega)$ vanishes above the edge, i.e., $A_c(\omega)=0$ for $\omega>0$ [Eq. (3.6)], it follows from this

relation that the same must be true for the exponent function $\alpha(\omega)$, i.e., $\alpha(\omega)=0$ for $\omega>0$, and we obtain the integral equation[51]

$$-\omega A_c(\omega)=\int_{\omega}^{0}\alpha(\omega-\omega')A_c(\omega')\,d\omega' \tag{3.22}$$

for the spectral function $A_c(\omega)$. With no frequency dependence in the exponent function, i.e., with $\alpha(\omega)=\alpha(0)$, this integral equation would be solved by the asymptotic expression (3.20) and we have the important relation

$$\alpha(0)=\alpha\ , \tag{3.23}$$

which explains the name "exponent function" for $\alpha(\omega)$. Furthermore, the frequency-dependent deviation of $\alpha(\omega)$ from its value at the edge measures the deviation of the spectral function from the asymptotic result. The usefulness of the exponent function $\alpha(\omega)$ stems from the fact that the asymmetry index α, obtained by fitting an asymptotic line shape (Eq. 3.20) with a variable α to a full ND spectrum, is approximately equal to the average of $\alpha(\omega)$ over the fitting region as will be discussed in Sec. V.

In practice, we solve the integral equation (3.12) for $G(0,t)$ and obtain $\alpha(\omega)$ from Eq. (3.21). The XPS line shape is then to be obtained either from the integral equation (3.22) or directely from Eq. (3.10), the two methods being equally convenient.

We end this section by noting an interesting sum rule. Owing to the sum rule (3.7) for the spectral function $A_c(\omega)$ we have from Eq. (3.22)

$$\int_{-\infty}^{0}\omega A_c(\omega)\,d\omega=-\int_{-\infty}^{0}\alpha(\omega)\,d\omega=-\Delta_r\ . \tag{3.24}$$

The last equality follows from the following considerations. Obviously, $\alpha(\omega)$ integrated over all frequencies is just $2\pi\alpha(t=0)$, which according to the Eqs. (3.16), (3.12), (3.13), and (2.6) is equal to

$$\beta-V_0\int_{\epsilon_F}^{\infty}A(\epsilon)\,d\epsilon=\Delta+V_0\int_{-\infty}^{\epsilon_F}A(\epsilon)\,d\epsilon$$
$$=\Delta+\langle N\mid V\mid N\rangle=\Delta_r\ .$$

Thus, the center of gravity of $A_c(\omega)$ falls at Δ_r below the edge. Shifting the edge back to the excitation energy of the core hole, the sum rule (3.24) is just a restatement of the well-known rule that the center of gravity of the excitation spectrum remains at the Hartree-Fock eigenvalue irrespective of the strength of the satellite structure. This rule is valid in ND theory as well as in the fully interacting case.[52] Of course, in the latter case the relaxation shift in a simple metal will have large contributions from the plasmon satellites in $A_c(\omega)$. Since ND theory does not account for these effects the corresponding "relaxation" shift is not relevant to real systems (cf. Ref. 44).

IV. RESULTS FOR SXE AND THE FINAL-STATE RULE

We start this section by establishing the usefulness of the determinantal finite-N approach. Consider for a moment the spectrum $J_1^{(N)}(\omega)$ obtained from this approach using N electrons in a box and including only single particle-hole pair excitations in the sum over final states prescribed by Eq. (2.7). This spectrum consists of discrete lines. However, as the number (N) of electrons is increased, $J_1^{(N)}(\omega)$ first approaches a continuous spectrum $J_1(\omega)$,[53] but eventually the spectrum collapses due to Anderson's orthogonality catastrophe,[33] i.e.,

$$\lim_{N\to\infty}J_1^{(N)}(\omega)=0\ .$$

The spectrum $J_2^{(N)}(\omega)$ obtained by also including double-pair excitations experiences a similar evolution with increasing N. It approaches a continuous spectrum $J_2(\omega)$, but, in this case, the final collapse occurs at a much larger N. Including several particle-hole pairs, N may be even larger before the integrated intensity of the corresponding spectrum tends to zero and the sequence $J_1(\omega),J_2(\omega),\ldots$ converges towards the exact spectrum $J(\omega)$ of the infinite system. As a matter of fact, we have, in the present paper, considered already $J_1(\omega)$ to be an accurate approximation to $J(\omega)$ but due to the computational difficulties associated with the inclusion of higher-order excitations, it is unfeasible to properly study the convergence properties of an asymptotic expansion as that described above. Fortunately, we are in a position to compare the approximate spectrum $J_1(\omega)$ directly with the result for the infinite system. Whereas the integral-equation approach in the simple version discussed here is limited to separable core-hole potentials, there is no restriction on the potential in the determinantal finite-N approach. In particular, we can compare results of the two methods using the same separable potential. Figure 1 shows such a comparison in the case of a separable core-hole potential of the form given by Eq. (2.25) with dipole matrix elements chosen to be

$$p_{ck}=\int e^{-\lambda r}\psi_k(r)\,d^3r\ . \tag{4.1}$$

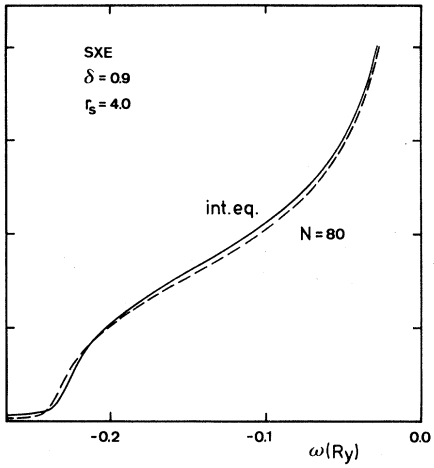

FIG. 1. Comparison between the emission spectra obtained for a separable potential from the integral-equation [Eq. (2.29)] formulation and from the determinantal finite-N approach ($N=80$).

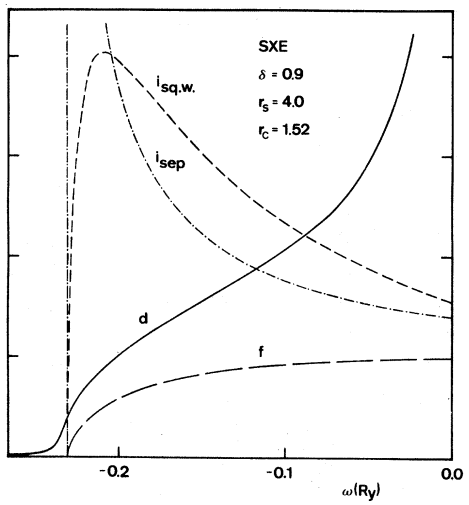

FIG. 2. The dynamical spectra (d) obtained in the finite-N approach for a spherical square-well potential (sq.w.) with radius r_c and a separable potential (sep) modeled to yield the same Fermi-level phase shift δ and the same integrated intensity of the static initial-state spectrum (i). Also shown is the static final-state spectrum (f).

The final-state wave functions $\{\psi_k\}$ are taken to be free spherical waves. In all emission examples presented here we have had in mind $L_{2,3}$ emission spectra which are determined essentially by the TDOS of s character. The core hole then has p symmetry but, in a picture based on orthogonalized plane waves, the energy dependence of the transition matrix element p_{ck} is, at small energies, mainly determined by the direct overlaps between plane waves and the lower-lying core states of s symmetry—in this case chosen to be a single $1s$ function with a reciprocal radius λ of 1.25 inverse Bohr radii. Thus, the choice given by Eq. (4.1) has the correct energy dependence at smaller energies. The potential parameter V_0 is -2.24 Ry giving a Fermi-level phase shift $\delta_F=0.90$. This phase shift as well as the density ($r_s=4$) of the free-electron gas used to simulate the ground-state solid both correspond approximately to sodium metal.[54] The spectrum from the finite-N approach is constructed using 80 s waves in a spherical box and the possible final states are limited to those having only a single excited particle-hole pair. The close agreement between this spectrum and that obtained for the infinite solid using the integral-equation approach is strong evidence for the rapid convergence of the asymptotic expansion discussed above. This comparison has also been performed in other cases corresponding to different choices of parameters and with the same encouraging results. Thus, Fig. 1 should be considered as a typical case and the present investigation represents the first strict demonstration of the usefulness of the finite-N approach.

Next, we intend to establish that the use of a separable potential does not give rise to any spurious results. As a matter of fact, a separable potential and a local potential, i.e., a potential depending only on position, give rise to very much the same dynamical ND spectra provided the parameters of the separable potential are chosen such that the Fermi-level phase shift and the integrated intensity of the resulting static initial-state spectrum are the same as for the local potential. This important fact, which is exemplified in Fig. 2, renders the simple one-dimensional version of the integral-equation approach quite useful for the calculation of dynamical ND spectra of real solids. The curve labeled f is the static final-state spectrum [Eq. (2.16)], i.e., the usual one-particle result with dipole matrix elements given by Eq. (4.1) in terms of free spherical waves. The curve marked $i_{\text{sq.w.}}$ is the static initial-state spectrum [Eq. (2.15)] for which the dipole matrix elements have again been obtained from Eq. (4.1) but this time using free spherical waves perturbed by a spherical square-well potential of radius $r_c=1.52$ Bohr radii and depth $V=-0.873$ Ry. The curve labeled i_{sep} is the static initial-state spectrum given by a separable potential determined as described at length in Sec. II [essentially from Eqs. (2.33), (2.34), (2.36), and (2.37)]. In particular, this potential gives the same

Fermi-level phase shift $\delta_F=0.90$ as the square-well potential and the area under the two curves labeled i_{sep} and $i_{sq.w.}$ is the same. The curve labeled d is the dynamical ND result obtained from the finite-N approach ($N=80$) using either of the two potentials. Therefore, this curve actually consists of two curves separated by less than 1%, which demonstrates the effective equivalence of the two potentials. We stress again that the results presented in the figures should be considered as typical and not merely as a consequence of fortuitous circumstances. Notice that the area under the dynamical curve is almost the same as under the two initial-state curves, the difference being due to the neglect of double-pair and higher-order excitations. This is a consequence of the sum rule Eq. (2.14) and explains why the separable potential was chosen so as to give the same integrated initial-state intensity as the square-well potential. As seen in Fig. 2 the difference in shape of the two initial-state spectra has, however, no effect on the resulting dynamical spectra which is a consequence of the final-state rule according to which the latter spectra reflect the spectral properties of the final state.

The accuracy of the final-state rule is the topic of the Figs. 3—9. According to this rule the dynamical ND spectrum $J(\omega)$ is well approximated by the formula

$$J(\omega)=CJ_f(\omega)\left[\frac{\epsilon_F}{\epsilon_F-\omega}\right]^{2\delta_F/\pi-\delta_F^2/\pi^2}, \qquad (4.2)$$

where $J_f(\omega)$ is the static final-state spectrum given by Eq. (2.16) and C is a constant which is determined by the sum rule (2.14) stating the equality of the integrated intensities of the dynamical and the static initial-state spectra. An approximate derivation of Eq. (4.2) is given in Sec. VI. The importance of the final-state rule derives from the fact that the rule *a posteriori* provides a justification for the numerous previous calculations of x-ray emission spectra based on band theory. The rule also shows how realistic x-ray emission and absorption[15] spectra may be obtained from simple one-particle theory without resorting to complicated dynamical calculations for realistic systems. Finally, the rule exactly corresponds to the commonly used procedure for obtaining threshold exponents from experimental emission spectra. This procedure is thus justified by the high accuracy of the final-state rule close to threshold. In Fig. 3 the spectrum from the final-state rule is compared to the full dynamical ND result chosen to be the same as in Figs. 1 and 2. In order to show the maximum deviation between the two spectra the constant C has here been chosen such that they agree at the Fermi level. Clearly the deviation at the bottom of the band is smaller than what can possibly be detected experimentally. It should be noted that the emission spectrum presented in Fig. 3 is representative of an emission spectrum in a simple metal, the Fermi energy and the corresponding phase shift approximating those found in sodium.[54] (Notice that the Fermi edge in all emission spectra has been placed at zero energy.)

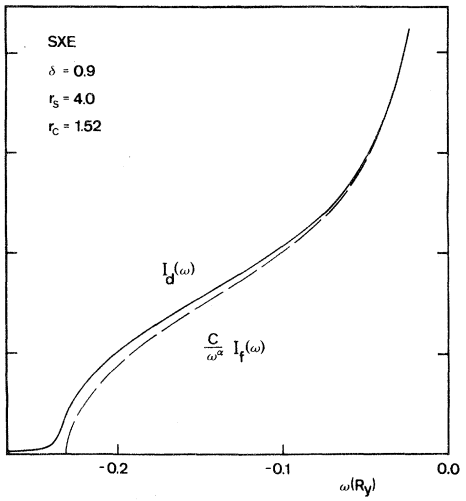

FIG. 3. Comparison between the dynamical spectrum obtained in the finite-N approach and the spectrum obtained from the final-state rule, where C was determined by fitting to the dynamical spectrum over the threshold region.

The only parameters in Eq. (4.2) which depend on the core-hole potential are the constant C and the Fermi-level phase shift δ_F. Therefore, the final-state rule implies that all core-hole potentials with the same phase shift will give rise to dynamical ND spectra of approximately the same shape. This prediction is tested in Fig. 4 showing ND spectra produced by three different square-well potentials with a common Fermi-level phase shift ($\delta_F=0.90$). The final-state spectrum, labeled f, is the same in all three cases and also the same as in Figs. 1—3 The static initial-state spectra indicated by the corresponding radii of the square wells are, however, quite different. Still, the resulting dynamical spectra are almost identical in shape. The weights of the initial-state spectra, i.e., their integrated intensities, differ by $\sim 10\%$. The dynamical spectra, here obtained from the finite-N approach ($N=80$), were, however, scaled to the

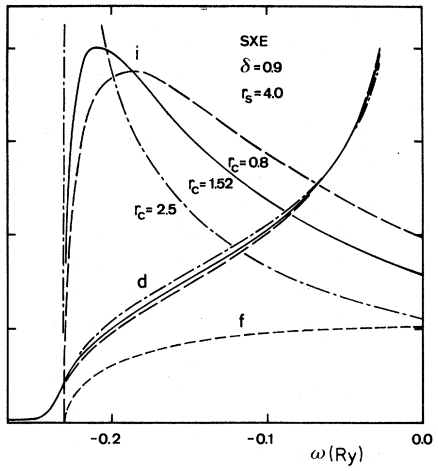

FIG. 4. Comparison between the dynamical spectra obtained in the finite-N approach for three square-well potentials with different radii r_c and whose depths were chosen to yield the same Fermi-level phase shift $\delta_F=0.9$. As the weights of the static initial-state spectra differed, the dynamical spectra were, for easier comparison, scaled to have the same weights.

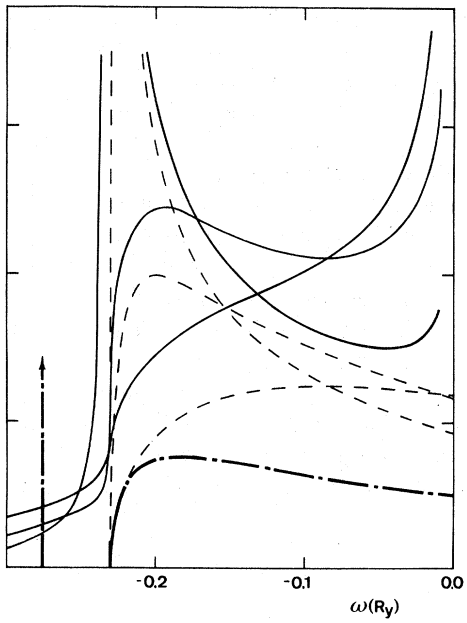

FIG. 5. The dynamical spectra (full drawn curves) for three systems characterized by the same static initial-state spectrum (heavily drawn, broken curve) with a bound state below the band and three different static final-state spectra (dashed curves).

same weight in order to facilitate the comparison of their shapes.

In order to demonstrate the usefulness of the final-state rule also for very strong core-hole potentials we show in Fig. 5 dynamical ND spectra from the integral-equation approach using a separable core-hole potential which is strong enough to pull a bound state out of the band. The position of the bound state is indicated by the vertical arrow in the static initial-state spectrum (dashed-dotted curve) which is chosen to be the same for all three cases shown. We have instead decided to vary the static final-state spectrum (dashed curves) by leaving an attractive impurity potential of variable strength in the final state of the emission process. The Fermi-level phase shifts of the residual impurity potentials in the three cases are 0.64, 0.33, and 0.00 and thus the first two cases correspond to emission from an impurity site in a simple metal. As a matter of fact, the parameters of the transition density of states are chosen such that the first case ($\delta_F=0.64$) simulates $L_{2,3}$ satellite emission in sodium. The initial state of this process has two core holes with a potential which causes a bound $3s$ state to drop out of the band.[6] The final state has only one core hole but the corresponding potential is still strong enough to cause a large buildup of oscillator strength of s character towards the bottom of the band. As shown by Fig. 5 there remains no trace of the bound state in any of the dynamical spectra (full curves) which rather closely resemble their respective final-state spectra (dashed curves), the difference being due to the threshold singularities and the shake-up structure below the band in the dynamical spectra. Figure 5 also demonstrates how the strengths of the singularity and the shake-up structure vary with the strength of the core-hole potential. As shown in Ref. 54 the Fermi-level phase shift of the core-hole potential is given by the difference between the phase shifts of the initial- and the final-state potentials. For the initial state we here have $\delta_F=1.01$ which in our three cases results in core-hole potentials having $\delta_F=0.37$, 0.68, and 1.01 with smaller phase shifts and thus weaker singularities and weaker shake-up structure being associated with more attractive final-state potentials.

In a rather recent letter,[29] Swarts, Dow, and Flynn, on the basis of the finite-N approach, presented numerical evaluations of the ND theory of emission and absorption spectra and they concluded that the spectra rather reflected the spectral properties of the initial state—at least for weaker core-hole potentials. For stronger potentials they stated that the dynamical spectra could not be described by either of the two static limits. These conclusions are, of course, at odds with everything

said so far in the present work. In order to resolve this controversy we have here repeated some of their calculations of emission spectra which were obtained by using a square-well core-hole potential in the free-electron gas. The results are shown in the Figs. 6–8 where, as before, *i*, *f*, and *d* label the static initial- and final-state spectra and the dynamical ND spectrum, respectively. Following Swarts *et al.*, we have here used the valence wave function at the origin as a measure of the core-valence dipole matrix element. This is the reason for the unphysically large ratio between the weights of the static initial- and final-state spectra, as discussed at the end of Sec. II. Above the spectra these figures also show an energy-dependent function $C(\omega)$, which is defined as

$$C(\omega)=\frac{J(\omega)}{J_f(\omega)}\left[\frac{\epsilon_F-\omega}{\epsilon_F}\right]^{2\delta_F/\pi-\delta_F^2/\pi^2} . \quad (4.3)$$

Thus, an energy independent $C(\omega)$ leads directly to Eq. (4.2) and the deviation of $C(\omega)$ from a horizontal line measures the deviation from the final-state rule. The very weak energy dependence that we find for $C(\omega)$ is strong evidence for the numerical accuracy of this rule. Only the strongest potential in Fig. 8 gave a minor deviation of the order of 10%,[55] and this potential is more attractive than those found in real simple metals. Note that $C(\omega)$ rapidly tends to infinity very close to the bottom of the band. This does not signal a deviation from the final-state rule but is merely a manifestation of the simple fact that the final-state spectrum vanishes at the band bottom whereas the dynamical spectrum, due to shake-up processes, is very small but finite. Thus, the results of Swarts, Dow, and Flynn accurately obey the final-state rule. The spectra in the Figs. 6–8 are quite dominated by the strong singularity at the Fermi edge. This unphysical result is due to the fact that only

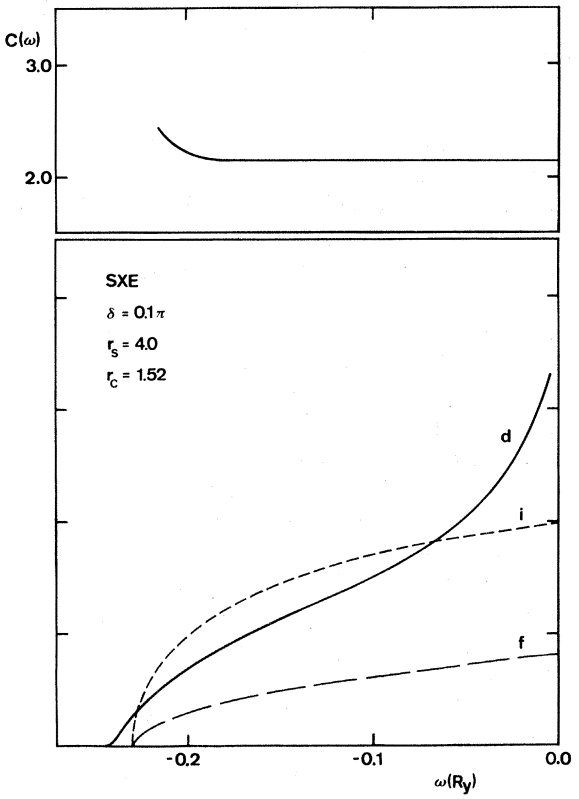

FIG. 6. The dynamical (*d*) emission spectrum obtained in the finite-N approach ($N=80$) for a square-well potential is compared to the corresponding initial (*i*) and final (*f*) state spectra. The deviation from a horizontal line of the function $C(\omega)$ defined in Eq. (4.3) measures the deviation from the final-state rule.

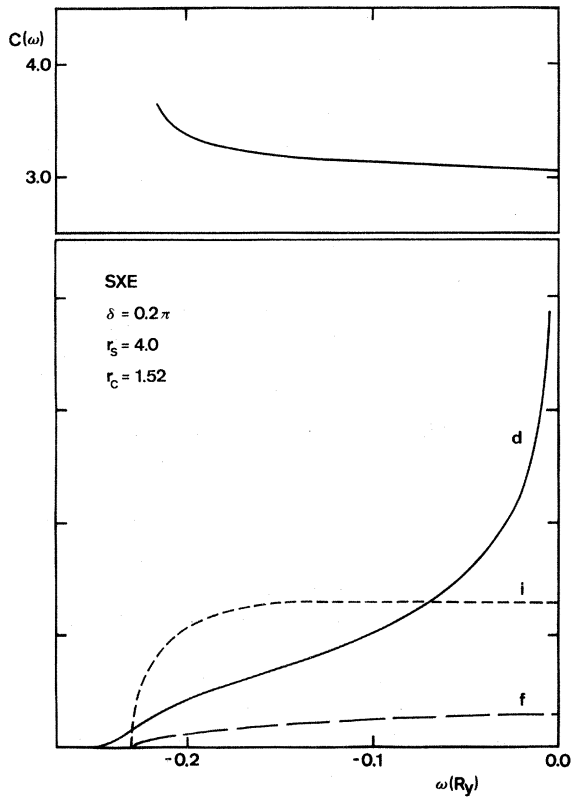

FIG. 7. The dynamical (*d*) emission spectrum obtained in the finite-N approach ($N=80$) for a square-well potential is compared to the corresponding initial (*i*) and final (*f*) state spectra. The deviation from a horizontal line of the function $C(\omega)$ defined in Eq. (4.3) measures the deviation from the final-state rule.

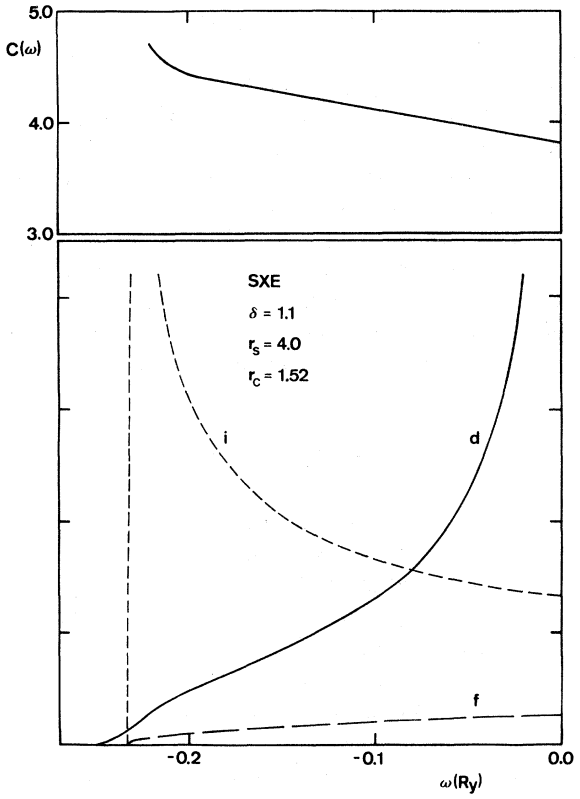

FIG. 8. The dynamical (d) emission spectrum obtained in the finite-N approach ($N=150$) for a square-well potential is compared to the corresponding initial (i) and final (f) state spectra. The deviation from a horizontal line of the function $C(\omega)$ defined in Eq. (4.3) measures the deviation from the final-state rule.

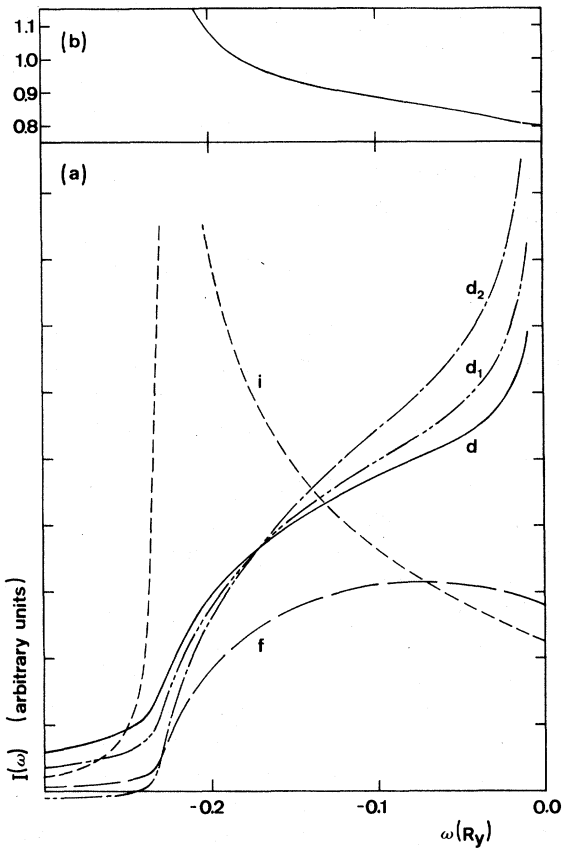

FIG. 9. (a) Comparison between the dynamical $L_{2,3}$ emission spectrum for sodium (d,d_1,d_2) and the static limits given by the initial (i) and final (f) state spectra. d_2: the threshold singularity is purely excitonic in nature: d_1: the threshold singularity is reduced by particle-hole excitations of s character; d: the threshold singularity is further reduced by particle-hole excitations also of p character. (b) The function $C(\omega)$ defined by Eq. (4.3).

one spin and angular-momentum channel is included. With the inclusion of all channels the singularity is strongly reduced (cf. Fig. 9) in accordance with the experimental facts, and the resemblance in shape between the dynamical and the final-state spectra becomes more apparent. It then becomes less important to analyze the calculated spectra in terms of Eq. (4.3) in order to realize the validity of the final-state rule. Note also that the initial-state spectrum and the dynamical spectrum have the same integrated weight [Eq. (2.14)]. Therefore, for weaker potentials without the strong resonance at the bottom of the band, one might be led to conclude an initial-state rule if undue importance is attached to absolute intensities which are not measured. The temptation to draw this conclusion is of course greater if there is an unphysically large ratio between the integrated intensities of the static initial- and final-state spectra. These points could perhaps explain the conclusions of Swarts *et al.*[29,56]

In Fig. 9 we present a realistic $L_{2,3}$ emission spectrum of sodium obtained from the integral-equation approach. As described at length in Sec. II the s and p angular-momentum channels of the static initial- and final-state spectra were fitted to the corresponding channels of the one-particle spectra obtained from fully self-consistent calculations for sodium with and without a core hole on one site.[6] The very small[6] d contribution to the spectrum was here neglected. The resulting Fermi-level phase shifts of s and p character (0.58 and 0.33) are somewhat different from those generally expected on the basis of theory[54] and XPS experiments.[37] They rather correspond to those, e.g., used by Callcott *et al.* in order to interpret their SXA experiment on sodium.[16] The resulting threshold exponent ($\alpha_0=0.23$) is intermediate be-

tween that used by Citrin[5] ($\alpha_0=0.38$) to fit the absorption data of Kunz[57] and that used by Callcott *et al.*[16] ($\alpha_0=0.15$) to fit their emission data. This ambiguity in the experimentally determined threshold exponents indicates that the physics of the x-ray edges is not yet fully understood. In particular, there is a need for further investigations of exchange effects and of the effects of valence-valence interactions not accounted for in the ND theory. Due to dipole selection rules only s electrons contribute to the static initial (i) and final (f) state spectra when d electrons are neglected. As seen in Fig. 9 the final-state spectrum (f) has a very smooth structureless appearance reflecting the almost parabolic s band of sodium, whereas the initial-state spectrum (i) shows a strong s resonance towards the bottom of the band due to the presence of the core hole. There is, however, no trace of this marked structure in the resulting dynamical ND spectrum whose shape rather resembles that of the final-state spectrum only multiplied by a threshold singularity. This is demonstrated in detail by the insert showing the energy variation needed in the "constant" C in order to make Eq. (4.2) an exact relation. Thus, the deviation from the final-state rule is only 10% over half the bandwidth, again demonstrating the numerical accuracy of the final-state rule. Note that a slightly slanting $C(\omega)$ will not affect the interpretation of experimental spectra in terms of the final-state rule since such an effect will probably be washed out by the background subtraction from the raw data. The curves labeled d_1 and d_2 in Fig. 9 explain why it is necessary to calculate also the p contribution to the transition density of states (TDOS). Whereas the initial- and final-state spectra and also the so-called transient Green's function $\tilde{G}(t;t)$ [cf. Eqs. (2.22) and (2.26)] are entirely determined by the TDOS of s character, the dynamical spectrum has contributions from all angular momentum and spin channels via the "overlap" function $\tilde{g}(t)$ [Eq. (2.24)]. This is due to the fact that the sum in Eq. (2.24) must be carried out over all quantum labels including magnetic and spin quantum numbers. The additional channels cause a reduction of the threshold exponent and of the threshold singularity. For instance, $2(\delta_F/\pi)-(\delta_F/\pi)^2$ in Eq. (4.2) becomes $2(\delta_0/\pi)-2\sum_l(2l+1)(\delta_l/\pi)^2$ in terms of the Fermi-level phase shifts δ_l of the lth angular momentum channel.[12] This effect is demonstrated in Fig. 9. The curve d_2 (Ref. 58) is the dynamical spectrum obtained without any orthogonality suppression of the threshold, i.e., using $\tilde{g}(t)=1$ in Eq. (2.27). The threshold exponent of this spectrum is $2\delta_0/\pi$. The curve d_1 is the dynamical spectrum obtained by including both spin channels of s symmetry giving a threshold exponent $2(\delta_0/\pi)-2(\delta_0/\pi)^2$. The curve d finally is the full dynamical spectrum obtained by also including all the p channels and the corresponding threshold exponent is $2\delta_0/\pi-2(\delta_0/\pi)^2-6(\delta_1/\pi)^2$ ($\delta_l\simeq 0$, $l\geq 2$). Figure 9 demonstrates that it is essential to include the higher angular-momentum channels in order to reduce the threshold singularity before a quanitative comparison with experiment is made.

V. RESULTS FOR XPS

The examination of the energy range over which the asymptotic power-law line shape of XPS is a close approximation to the full result of ND theory is, as noted in Sec. III, done best by inspecting the exponent function $\alpha(\omega)$ [Eq. (3.21)]. In this way one avoids the difficult task of directly comparing two singular functions.[51] It also becomes redundant to accurately determine the normalization constant of the asymptotic theory [Eq. (3.20)] which depends on the potential in a more complicated way than simply through the Fermi-level phase shift δ_F and whose uncertainty has been a problem in previous investigations.[40] As described in Sec. III, the determinantal approach leads immediately to the XPS spectrum [Eq. (3.8)], but in this approach $\alpha(\omega)$ can only be obtained indirectly from a somewhat inaccurate fitting procedure based on Eq. (3.22). In Fig. 10 we show $\alpha(\omega)$ for the case of $N=100$ free s electrons in a box with a density corresponding to sodium ($r_s=4$) and a core-hole potential simulated by a square-well potential yielding a Fermi-level phase shift $\delta_F=1.3$. Notice that the exponent at the edge is determined by $\alpha(\omega)$ at $\omega=0$ [Eq. (3.23)], i.e., at the left in Fig. 10. It is obvious from Eq. (3.22) that an $\alpha(\omega)$ which is constant over a certain range of energies away from the edge will yield a spectral function $A_c(\omega)$ which follows an exact power law within this range. However, any structure in $\alpha(\omega)$ will yield a corresponding structure in $A_c(\omega)$. In Fig. 10 we see that $\alpha(\omega)$ indeed remains rather constant over an appreciable fraction of the occupied bandwidth. A fit to the corresponding spectral function over this range will disclose a very accurate power-law behavior. The obtained exponent will be some weighted mean of $\alpha(\omega)$ over this range and the variation of $\alpha(\omega)$ will set the error bar for the

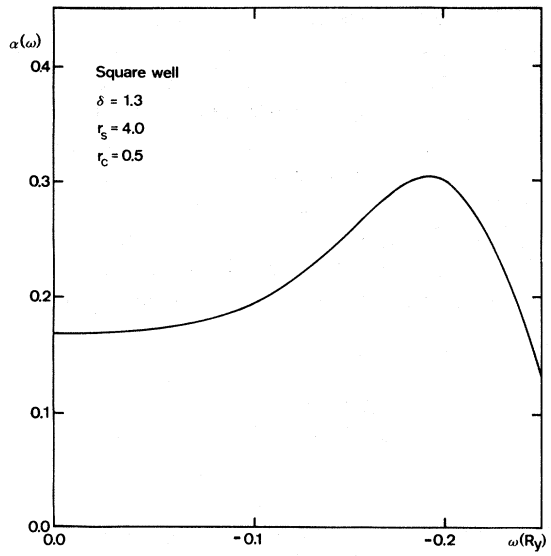

FIG. 10. The exponent function $\alpha(\omega)$ obtained from the determinantal approach for $N=100$ free s electrons with a density corresponding to that of sodium.

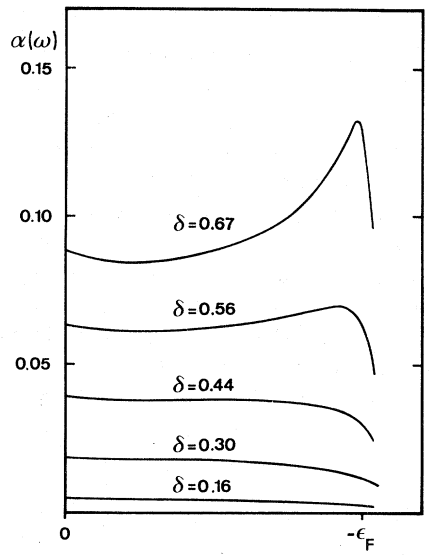

FIG. 11. The exponent function $\alpha(\omega)$ obtained from the integral-equation approach for a model system with five separable potentials of different strengths. The Fermi level is placed at the middle of a semielliptic DOS.

extracted exponent. For energies of the order of the Fermi energy ($\epsilon_F=0.23$ Ry) away from the edge, one notes a broad peak which is a consequence of the high probability for particle-hole excitations with an energy $\sim\epsilon_F$ due to the strong resonance at the bottom of the band (cf., e.g., Fig. 2), when it is calculated in the presence of the core hole. This structure has, however, only a minor effect on the spectral function, as the latter has become rather small this far from the edge. The spectral function is actually quite insensitive to variations in $\alpha(\omega)$ away from the edge. It should be noted that the phase shift of this system is larger than any value experimentally predicted or theoretically calculated for simple metals and would by itself almost exhaust Friedel's sum rule. In Fig. 11 we show exponent functions obtained fom the intergral-equation approach for a model system and five different separable core-hole potentials. The density of states was chosen to be a semielliptic band with ϵ_F at half the bandwidth. The structure in $\alpha(\omega)$ at energies $\sim\epsilon_F$ away from the edge is here slightly sharper, reflecting the sharper peak in the density of states obtained in the presence of a separable core-hole potential (cf., e.g., Fig. 2). The overall trend, however, agrees with the result of Fig. 10, $\alpha(\omega)$ again being closely constant over about half the bandwidth. Both a square-well and a separable potential thus yield a similar behavior of $\alpha(\omega)$. Thus, in these systems, we find an asymptotic power-law behavior over a substantial fraction of the bandwidth away from the edge and we conclude that singularity indices may be rather accurately determined by fitting to experiment (see also the discussion below). These findings are at odds with what has been claimed by Dow *et al.*[40] Of course, cases may be constructed, either by distorting the density of states far from the free-electron behavior it has in simple metals or by applying excessively strong potentials, where the deviation of $\alpha(\omega)$ from a constant may be strong already at small energies. Such cases are, however, not relevant for the present discussion of simple metals.

In Fig. 12 we show the exponent function $\alpha(\omega)$ for the system which we discussed at length in Sec. IV in connection with Fig. 9 and which was chosen to closely model sodium. Also shown is the angular-momentum decomposition into the

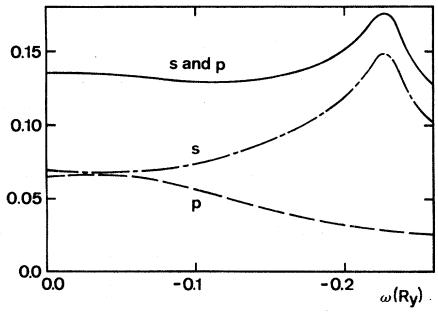

FIG. 12. The exponent function $\alpha(\omega)$ for a system chosen to model sodium. Also shown is the decomposition into individual angular momentum channels.

dominant s and p channels. While $\alpha(\omega)$ for both individual channels varies by almost 20% over half the bandwidth, the sum remains much more closely constant. In order to determine the effect of a varying $\alpha(\omega)$ on the commonly used procedure to determine the assymmetry index from the measured XPS line shape,[37] we decided to consider the individual angular momentum and spin components of $\alpha(\omega)$ in sodium as examples of possible energy-dependent exponent functions in F simple metals. The exact ND spectral function obtained by solving the integral equation (3.22) with $\alpha(\omega)$ given by one of these components, was broadened by a Gaussian and a Lorentzian with full width at half-maximum values of 0.023 and 0.003 Ry, respectively. The Lorentzian width, reflecting the lifetime of the core hole and the Gaussian width, reflecting phonon broadening, were chosen to values typical for XPS spectra of shallower core holes in simple metals.[37] In an attempt to retrieve the input parameters, the resulting spectrum was then fitted by a broadened version of the asymptotic form [Eq. (3.20)] by taking the two broadenings, the exponent, the threshold position, and the normalization as variational parameters. This defines the commonly used procedure for obtaining asymmetry indices from experimental spectra. The best fit was determined by minimizing the sum of the squared differences between the two spectra taken at equidistant points, 0.01 Ry apart, over varying fitting ranges. The result is given in Table II and shows the remarkable accuracy with which both the Lorentzian and the Gaussian broadenings could be determined. The accuracy of the extracted threshold exponent is actually somewhat better than the accuracy claimed from experiment. We thus conclude that even variations in the exponent function $\alpha(\omega)$, which are stronger than those likely to be found in simple metals, do not significantly affect the accuracy by which the asymmetry indices can be obtained from experiment. It should be remembered that this conclusion is based entirely on the ND theory which does not account for the interaction between the valence electrons. There is, however, yet no evidence indicating that the interaction effects might modify our conclucion. On the contrary, an investigation by Minnhagen[35] based on the theory of XPS derived by Langreth[59] indicates that the electron-electron interactions serve to make the XPS line shape more asympotic.

VI. APPROXIMATE DERIVATION OF THE FINAL-STATE RULE

In this section we will present an approximate though rather accurate description of emission spectra from which the final-state rule becomes rather evident. The discussion is based on the determinantal approach. In Sec. IV we demonstrated that, in simple metals, this approach gives the correct answer to within $\sim 5\%$ already with rather small determinants ($N \sim 100$) and including only single-pair excitations which are given by the first two lines of Eq. (2.12). In order to obtain an expression for the emission spectrum which can be evaluated analytically, we introduce the further approximation of restricting the electron of the excited electron-hole pair to be at the Fermi level. We then obtain

$$J(\omega)=\sum_k |\langle N\sim | b^\dagger a_k | N\rangle|^2 \delta(\omega-\epsilon_k) . \quad (6.1)$$

Thus, this approximation simply corresponds to restricting the final states to be of the form $c^\dagger a_k | N\rangle$, i.e., Slater determinants consisting of one-particle orbitals evaluated in the final-state potential and having a single hole below the Fermi level. All shake-up processes are thus neglected.

In the case of a free-electron gas with a core-

TABLE II. Threshold exponents and broadenings determined by assuming different ranges of validity of the asymptotic line shape.

	s channel			p channel		
Fitting range[a]	α	Γ_{Lor}	Γ_{Gau}	α	Γ_{Lor}	Γ_{Gau}
0.00−0.04	0.0336	0.00299	0.0233	0.0113	0.00300	0.0233
−0.04−0.04	0.0334	0.00300	0.0233	0.0112	0.00300	0.0233
−0.12−0.04	0.0338	0.00301	0.0233	0.0107	0.00299	0.0233
−0.20−0.04	0.0345	0.00297	0.0233	0.0102	0.00300	0.0233
Exact values	0.0338	0.00300	0.0233	0.0111	0.00300	0.0233

[a]The end points of the fitting region are given in Rydbergs relative to the threshold position.

hole potential approximated by a square-well potential with a Fermi-level phase shift δ_F equal to 1.1, we have found numerically that this simple approximation gives an emission spectrum which is accurate to within 15% when $N=80$. This chosen potential is probably stronger than the actual core-hole potential of any simple metal and the approximation quickly improves as the Fermi-level phase shift is reduced. When $\delta_F=0.2\pi$, the error is only 6%. Since there are no shake-up processes, the approximation (6.1) cannot account for the orthogonality suppression[33] of the emission threshold, and we thus expect Eq. (6.1) to give a spectrum with an exaggerated threshold singularity and too little intensity towards the bottom of the band. The main effect of the shake-up terms is, however, similar to a convolution with a power-law singularity. They are only important at threshold and Eq. (6.1) gives a sufficiently accurate description of the general shape of the emission band to allow us to demonstrate the final-state rule in a qualitative way.

Inserting the expression (2.5) for the creation operator $b^\dagger$ of the transition orbital into Eq. (6.1), we obtain

$$J(\omega)=\sum_k |\rho p_{ck}+\sum_\mu p_{c\mu}\beta_{\mu k}|^2\delta(\omega-\epsilon_k) \tag{6.2}$$

in terms of the coefficients

$$\rho=\langle N|N\sim\rangle \tag{6.3}$$

and

$$\beta_{\mu k}=\langle N|a_k^\dagger a_\mu|N\sim\rangle\ . \tag{6.4}$$

Notice that greek and latin letters denote states above and below the Fermi level, respectively. Due to the completeness of the set of Slater determinants constructed from a complete set of one-particle states, the ground state $|N\sim\rangle$ obtained in the presence of the core hole can be expanded according to

$$|N\sim\rangle=\rho|N\rangle+\sum_{\mu,k}\beta_{\mu k}a_\mu^\dagger a_k|N\rangle + \sum_{\mu,\nu,k,l}\gamma_{\mu\nu,kl}a_\mu^\dagger a_\nu^\dagger a_k a_l|N\rangle+\cdots\ . \tag{6.5}$$

Thus, the approximation (6.1) can alternatively be viewed as a truncation of this expansion after the term corresponding to single-pair excitations which should be an adequate procedure when the core-hole potential is not too strong. The overlap ρ is obviously equal to $\det S^{(N)}$, where $S^{(N)}$ is the overlap matrix involving only occupied states [cf. Eq. (B4)]

$$S_{kk'}^{(N)}=\langle k|k'\sim\rangle,\quad \epsilon_k,\epsilon_{k'}\le\epsilon_F\ . \tag{6.6}$$

The coefficient $\beta_{\mu k}$, on the other hand, is the determinant obtained from $S^{(N)}$ by replacing the kth row by the numbers $\langle\mu|k'\sim\rangle$, $\epsilon_{k'}\le\epsilon_F$. Thus, expanding this determinant along the kth row we obtain

$$\beta_{\mu k}=\det S^{(N)}\sum_{k'}\langle\mu|k'\sim\rangle S_{k'k}^{(N)-1} \tag{6.7}$$

in terms of the inverse $S^{(N)-1}$ of the overlap matrix $S^{(N)}$. At this stage we find it convenient to introduce a continuum approximation and convert discrete sums to integrals. For this purpose we rewrite Eq. (6.7) as

$$\sum_{k'}\beta_{\mu k'}S_{k'k}=\rho S_{\mu k} \tag{6.8}$$

and use the expression for $S_{kk'}$ derived in Appendix B [Eq. (B15)]

$$\beta_{\mu k}+\frac{1}{\pi}\tan\delta_k\frac{p_{ck}}{A(\epsilon_k)}\sum_{k'}\frac{\beta_{\mu k'}p_{ck'}^*}{\epsilon_{k'}-\epsilon_k} =\rho\frac{1}{\pi}\tan\delta\frac{p_{ck}}{A(\epsilon_k)}\frac{p_{c\mu}^*}{\epsilon_\mu-\epsilon_k}\ . \tag{6.9}$$

Defining the auxiliary quantity γ_k as

$$\gamma_k=\mathscr{D}(\epsilon_k)p_{ck}^*\sum_\mu p_{c\mu}\beta_{\mu k} \tag{6.10}$$

and converting sums over k and μ to integrals over the corresponding energy intervals, we obtain the following integral equation for $\gamma(\epsilon)$:

$$\gamma(\epsilon)+\frac{1}{\pi}\tan\delta(\epsilon)\int_{-\infty}^{\epsilon_F}\frac{\gamma(\epsilon')}{\epsilon'-\epsilon}d\epsilon' =\frac{\rho}{\pi}\tan\delta(\epsilon)\int_{\epsilon_F}^{\infty}\frac{A(\epsilon')}{\epsilon'-\epsilon}d\epsilon'\ . \tag{6.11}$$

Notice that the overlap ρ tends to zero in the continuum limit $N\to\infty$. The decay is, however, governed by the formula[33]

$$\rho^2=\rho_0^2N^{-(\delta_F/\pi)^2}\ .$$

It is thus rather slow (the columns marked S_0 in Table I show the dependence of ρ^2 on N) and ρ is still appreciable when the solution to the continuous integral equation (6.11) represents an accurate approximation to the discrete problem given by Eq. (6.7). As noted above, Eq. (6.2) yields a rather accurate spectrum with as many as 80 s waves in a box and in this case the level spacing is small enough for the continuum approximation to be re-

liable. It should be remembered that this approximation is merely a convenient tool which permits us to penetrate the mechanisms leading to the results of the determinantal approach.

As demonstrated in Appendix C, the seemingly complicated integral equation for $\gamma(\epsilon)$ can actually be solved analytically using a method due to Muskhelishvili[60] and the result is

$$\gamma(\epsilon)=\frac{\rho}{\pi}\frac{A(\epsilon)}{\eta(\epsilon)}\int_{\epsilon_F}^{\infty}\frac{\eta(\epsilon')\sin\delta(\epsilon')}{\epsilon'-\epsilon}\,d\epsilon' \tag{6.12}$$

in terms of the function

$$\eta(\epsilon)=\exp\left[\frac{1}{\pi}\int_{\epsilon_F}^{\infty}\frac{\delta(\epsilon')}{\epsilon-\epsilon'}\,d\epsilon'\right]. \tag{6.13}$$

Remembering that the final-state spectrum $J_f(\omega)$ is just the occupied part of the TDOS $A(\omega)$ obtained in the absence of the core hole [Eq. (2.34)], we can combine the Eqs. (6.2), (6.10), (2.32), and (6.12) in order to express the approximate dynamical ND spectrum $J(\omega)$ in terms of the static final-state spectrum $J_f(\omega)$,

$$J(\omega)=\rho^2 J_f(\omega)\left[1+\frac{1}{\pi\eta(\omega)}\int_{\epsilon_F}^{\infty}\frac{\eta(\epsilon)\sin\delta(\epsilon)}{\epsilon-\omega}\,d\epsilon\right]^2. \tag{6.14}$$

In Fig. 13 we compare the spectrum obtained from a direct numerical evaluation of this formula and the spectrum obtained from the integral-equation approach with a separable potential having a phase shift $\delta_F=0.90$. The similar shapes of the two spectra suggest that our approximate treatment is sufficiently accurate to allow us to use it for a qualitative derivation of the final-state rule. In order to study the behavior of the function $\eta(\epsilon)$ we introduce an energy cutoff ϵ_0 in the integral in Eq. (6.13) and obtain

$$\eta(\epsilon)=\left|\frac{\epsilon-\epsilon_F}{\epsilon-\epsilon_0}\right|^{\delta_F/\pi}, \quad |\epsilon-\epsilon_F|\to 0. \tag{6.15}$$

Thus, towards the Fermi level, the function $\eta(\epsilon)$ tends to zero, whereas the inverse which appears in Eq. (6.14) has a power-law singularity with exponent δ_F/π. Directly from the defining equation we see that $\eta(\epsilon)$ is everywhere positive and that it tends to unity at large energies. Towards the bottom of the band it tends to a constant of order $\exp(-2\delta_F/\pi)<1$. From these properties and from the fact that the phase shift above ϵ_F is usually a slowly varying function which tends to zero as $\epsilon^{-1/2}$, it follows that the integral in Eq. (6.14) gives rise to a monotonically increasing function which actually is small, typically of the order of 0.1, at the bottom of the band and which reaches a value of the order of unity at the Fermi level. Consequently, the entire enhancement factor defined as the ratio of the dynamical spectrum and the final-state spectrum, i.e., ρ^2 times the square in Eq. (6.14), has a smooth behavior, tending to a constant of order unity towards the bottom of the band and exhibiting a power-law singularity at the Fermi energy with a threshold exponent equal to $2\delta_F/\pi$. As a matter of fact, the enhancement factor is quite well represented by the simple expression

$$C(\omega)\left[\frac{\epsilon_F}{\epsilon_F-\omega}\right]^{2\delta_F/\pi},$$

where the function $C(\omega)$ is almost constant over the entire occupied band. We thus have the approximate result

$$J(\omega)=CJ_f(\omega)\left[\frac{\epsilon_F}{\epsilon_F-\omega}\right]^{2\delta_F/\pi} \tag{6.16}$$

in terms of a known but irrelevant constant C. This is the final-state rule for emission disregarding shake-up effects. As mentioned previously, such effects are not included in the simple approximation given by Eq. (6.1) which, however, correctly describes the excitonic enhancement[32] of the threshold as is evident from Eq. (6.16). In the

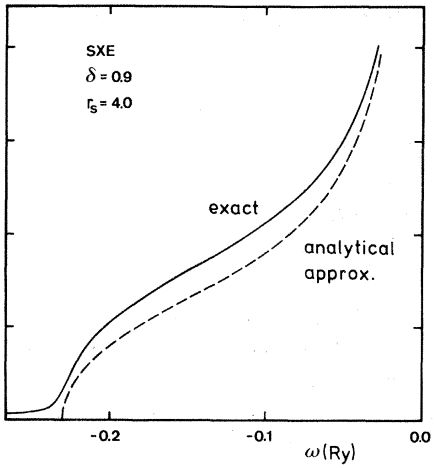

FIG. 13. Comparison between the emission spectra obtained for a separable potential from the integral-equation approach and from the approximate expression, Eq. (6.14).

time representation the shake-up effects enter [cf. Eq. (2.21)] the ND theory via the multiplicative factor $\tilde{g}(t)$ given by Eq. (2.24). Therefore, these effects should really be accounted for via a convolution in frequency space. However, close to threshold the Fourier transform of $\tilde{g}(t)$ behaves as

$$(\epsilon_F-\omega)^{(\delta_F/\pi)^2-1},$$

leading to the suppression of the edge due to the Anderson orthogonality catastrophe.[33] Thus, close to threshold the distinction between convoluting with this expression or multiplying by

$$(\epsilon_F-\omega)^{(\delta_F/\pi)^2}$$

becomes irrelevant and we have found numerically that over most of the occupied band the shake-up effects are well accounted for by merely changing the exponent in Eq. (6.16) to $2(\delta_F/\pi)-(\delta_F/\pi)$.[2] Of course, at the very bottom of the band the final-state spectrum vanishes, whereas the dynamical spectrum is finite if shake-up effects are included. Therefore, the exact enhancement factor blows up close to the band bottom, a tendency which is apparent from Figs. 6–9. Disregarding this minor effect the final-state rule reads

$$J(\omega)=CJ_f(\omega)\left[\frac{\epsilon_F}{\epsilon_F-\omega}\right]^{2\delta_F/\pi-\delta_F^2/\pi^2} \tag{4.2}$$

VII. CONCLUSIONS

The final-state rule was established by the authors in 1977. The rule states that, disregarding the singular Fermi edges, accurate x-ray emission and absorption spectra of simple metals may be obtained from ordinary one-electron theory provided the relevant dipole matrix elements are calculated from valence wave functions obtained in the potential of the final state of the x-ray process, i.e., a potential reflecting the fully screened core hole in absorption but not in emission. The final-state rule was also modified[15] to include even the singular threshold behavior [Eq. (4.2)] which can be accurately accounted for via power-law factors with properly chosen exponents, one for each angular-momentum component of the spectrum. The importance of the final-state rule stems from the fact that this rule *a posteriori* provides a justification for the numerous earlier calculations of x-ray emission spectra based on band theory. The rule also shows how to obtain realistic x-ray emission and absorption spectra without resorting to complicated many-body calculations for real solids. Finally, the rule corresponds exactly to the commonly used procedure for obtaining threshold exponents from measured x-ray emission spectra. Thus, the accuracy of the final-state rule provides strong support for this procedure.

In the present paper we have made an extensive investigation of the validity of the final-state rule. This investigation is based entirely on the theory of x-ray spectra due to Nozières and DeDominicis.[12] For numerous realistic model systems including cases where the core-hole potential is strong enough to pull a bound state out of the band, we evaluate the ND theory numerically and show that the resulting dynamical ND emission spectra accurately obey the final-state rule. In fact, to date, no case is known for which the ND spectrum does not follow the final-state rule rather closely. In Sec. VI we present an approximate version of the ND theory for emission spectra which can be evaluated analytically and which leads naturally to the final-state rule. This approximate theory also gives some insight into the mechanisms behind the rule. For the numerical evaluations of the ND theory we have used two different methods, namely, the integral-equation approach originally suggested by Nozières and DeDominicis[12] and the determinantal finite-N approach first discussed by Friedel.[30] The integral-equation approach pertains to an infinite system, while the finite-N approach is based on a finite number (N) of electrons enclosed in a finite volume. In the limit of large N we show here both formally and numerically that the two methods are equivalent. In fact, by directly comparing the two methods we are able to prove that the finite-N approach gives rather accurate results already with an unexpectedly small number of particles ($N\sim 100$), thus rendering this approach quite useful for the calculation of x-ray and x-ray photoemission spectra. The approach based on the integral equation is greatly facilitated by the use of a separable core-hole potential and in our applications we have always taken advantage of this possibility. By directly comparing to the finite-N approach, which can treat all potentials with equal ease, we show here that a separable potential does not give rise to any spurious results. In fact, we show that any square-well potential and probably also any reasonable local potential can be effectively simulated by a separable potential. If the parameters of the separable potential are chosen such that this potential and the square well yield

the same Fermi-level phase shift and the same integrated intensity of the static spectrum obtained in the presence of the core hole, then the two potentials give rise to almost the same dynamical ND emission spectra. Thus, the approach based on the integral equation in connection with a separable core-hole potential is also a very useful tool for obtaining x-ray spectra in realistic systems.

In the present work we also discuss at length the application of the ND theory to XPS. According to the asymptotic version of this theory the XPS line shape close to the edge follows a power law. This fact forms the basis for the fitting procedure commonly used for extracting exponents from the measured XPS line shapes. The validity of this procedure thus relies on the validity of the asymptotic theory over the fitting range. We analyze here the full ND result for the XPS line shape in terms of the exponent function $\alpha(\omega)$, whose deviation from a constant measures the deviation of the asymptotic ND theory from the full ND theory. This procedure avoids the difficulties associated with a direct comparison of two singular spectra as well as the ambiguous choice of normalization constant which has sometimes been a problem in other treatments.[40] We present here results for the exponent function $\alpha(\omega)$ for several model systems which are chosen to correspond closely to real simple metals and we find that $\alpha(\omega)$ is indeed rather constant over about half the bandwidth away from the edge. We also study the effect of a varying $\alpha(\omega)$ by applying the fitting procedure to broadened versions of XPS spectra obtained from exponent functions with a rather strong variation with energy. The extracted asymmetry indices and broadenings were found to be very close to their correct values demonstrating the insensitivity of the extracted parameters to deviations from the asymptotic theory. These findings provide strong support for the accuracy of the commonly used fitting procedure.

Whereas the x-ray emission spectra of simple metals are dominated by electrons of a particular angular-momentum symmetry, the asymmetries of the XPS lines are strongly affected by particle-hole excitations of both s and p character. This is demonstrated here in the case of sodium by analyzing the exponent function $\alpha(\omega)$ into its angular-moment components. Since these particle-hole excitations act to reduce the threshold singularities of x-ray spectra, we show here that it is essential to include this effect before a detailed comparison is made between dynamical ND spectra and experiment.

In several papers[25,29,40,41] Dow and co-workers have reached conclusions which are contradictory to the main results of the present paper. We find that this investigation strongly supports the conclusions presented here and in previous work.[6,9,14,15].

ACKNOWLEDGMENTS

We wish to thank C.-O. Almbladh and L. Hedin for stimulating discussions during the course of this work. We also thank D. Langreth for critical reading of the manuscript and for helpful suggestions.

APPENDIX A

Following work by Langreth,[43] we will here give an elementary derivation of the basic integral equation of the original ND theory.[12] We wish to compute the correlation function $\tilde{F}_{kk'}(t)$ for negative times ($t \leq 0$). To this end we introduce a dummy variable τ into $\tilde{F}_{kk'}$:

$$\tilde{F}_{kk'}(\tau;t)=\langle N\sim | \tilde{a}_{k'}^{\dagger} e^{iH\tau}\tilde{a}_k e^{iH(t-\tau)}e^{-i\tilde{H}t} | N\sim \rangle \ , \tag{A1}$$

in such a way that $\tilde{F}_{kk'}(t)=\tilde{F}_{kk'}(t;t)$, and take the derivative with respective to τ,

$$i\partial_\tau \tilde{F}_{kk'}(\tau;t) = \langle N\sim | \tilde{a}_{k'}^{\dagger} e^{iH\tau}[\tilde{a}_k,H]e^{iH(t-\tau)}e^{-i\tilde{H}t} | N\sim \rangle \ . \tag{A2}$$

The commutator is obtained from the expression for the no-hole Hamiltonian H in terms of the core-hole basis [Eq. (2.11)]

$$[\tilde{a}_k,H]=\epsilon_k\tilde{a}_k-\sum_q \tilde{V}_{kq}\tilde{a}_q \ , \tag{A3}$$

which leads to a closed equation for $\tilde{F}_{kk'}(\tau;t)$

$$(i\partial_\tau-\epsilon_k)\tilde{F}_{kk'}(\tau;t)=-\sum_q \tilde{V}_{kq}\tilde{F}_{qk'}(\tau;t) \ . \tag{A4}$$

It is not difficult to see that the free-particle Green's function defined in Eq. (2.23) is an ordinary Green's functions for this first-order differential equation and we have

$$(i\partial_\tau-\epsilon_k)\tilde{G}_k^0(\tau)=\delta(\tau) \ . \tag{A5}$$

After multiplying Eq. (A4) by $\tilde{G}_k^0(\tau'-\tau)$, integrating by parts and interchanging dummy variables τ and τ', we obtain

$$\tilde{F}_{kk'}(\tau;t)=i\tilde{G}_k^0(\tau-t)\tilde{F}_{kk'}(t;t) -i\tilde{G}_k^0(\tau)\tilde{F}_{kk'}(0;t) +\sum_q\int_0^t d\tau'\tilde{G}_k^0(\tau-\tau') \times\tilde{V}_{kq}\tilde{F}_{qk'}(\tau';t) . \quad \text{(A6)}$$

Now, clearly from the definition, Eq. (2.20), the state k in $\tilde{F}_{kk'}(t)=\tilde{F}_{kk'}(t;t)$ must be occupied. We are, however, only interested in times $t\leq\tau\leq 0$ [Eq. (A6)]. Therefore, from Eq. (2.23), $\tilde{G}_k^0(\tau-t)=0$, and the first term of this equation vanishes. Since $\tau\leq 0$, the definition of $\tilde{G}_k^0(\tau)$ requires k to label an occupied state also in the second term of this equation, which leads to

$$n_k\tilde{F}_{kk'}(0;t)=n_k\langle N\sim|\tilde{a}_{k'}^\dagger\tilde{a}_k e^{iHt}e^{-i\tilde{H}t}|N\sim\rangle =n_k\delta_{kk'}\langle N\sim|e^{iHt}e^{-i\tilde{H}t}|N\sim\rangle . \quad \text{(A7)}$$

Consequently, the quantity $\tilde{g}(t)$ defined by

$$\tilde{g}(t)=\langle N\sim|e^{iHt}e^{-i\tilde{H}t}|N\sim\rangle \quad \text{(A8)}$$

must be a factor in $\tilde{F}_{kk'}(\tau,t)$ and by defining the auxiliary quantity

$$\tilde{G}_{kk'}(\tau;t)=i\tilde{F}_{kk'}(\tau,t)/\tilde{g}(t) \quad \text{(A9)}$$

we obtain the integral equation (2.22). This equation evidently determines $\tilde{G}_{kk'}(\tau,t)$ in the entire interval $t\leq\tau\leq 0$, but we still need $\tilde{g}(t)$ in order to find $\tilde{F}_{kk'}(t)$. From Eqs. (A1), (2.10), and (2.11) we obtain

$$\sum_{k,k'}\tilde{V}_{k'k}\tilde{F}_{kk'}(0;t)=\langle N\sim|Ve^{iHt}e^{-i\tilde{H}t}|N\sim\rangle =i\partial_t\langle N\sim|e^{iHt}e^{-i\tilde{H}t}|N\sim\rangle , \quad \text{(A10)}$$

where we have used the fact that $|N\sim\rangle$ is an eigenstate of $\tilde{H}$ to obtan the second equality. Thus,

$$\tilde{g}(t)\sum_{k,k'}\tilde{V}_{k'k}\tilde{G}_{kk'}(0;t)=-\partial_t\tilde{g}(t) \quad \text{(A11)}$$

and since $\tilde{g}(0)=1$ [Eq. (A8)], this differential equation has the solution given by Eq. (2.24).

APPENDIX B

We will show here how the transition density of states (TDOS) in the presence of a core hole is obtained from that of the ground state when the core-hole potential has the separable form given by Eq. (2.25). From the definitions of the TDOS's, Eqs. (2.31) and (2.32), we obviously need the dipole matrix elements $\tilde{p}_{ck}$ and p_{ck} with and without the core-hole and the corresponding one-particle states $|k\sim\rangle$ and $|k\rangle$. These are eigenstates of the one-particle Hamiltonians $\tilde{H}$ and H defined by the Eqs. (2.8) and (2.9). Thus,

$$H|k\rangle=\epsilon_k|k\rangle , \quad \text{(B1)}$$

$$\tilde{H}|k\rangle=\tilde{\epsilon}_k|k\sim\rangle , \quad \text{(B2)}$$

where the eigenvalues are assumed to be in the continuum. Since the perturbing potential $V=\tilde{H}-H$ has a finite range, the eigenvalues can also be assumed to be equal, $\tilde{\epsilon}_k=\epsilon_k$. The eigenstates of H form a complete set and we have

$$\tilde{p}_{ck}=\sum_{k'}p_{ck'}S_{k'k} \quad \text{(B3)}$$

in terms of the overlap matrix S defined by

$$S_{kk'}=\langle k|k'\sim\rangle . \quad \text{(B4)}$$

The overlap matrix is easily obtained directly from the eigenvalue expressions (B1) and (B2)

$$S_{kk'}=\frac{\langle k|V|k'\sim\rangle}{\epsilon_{k'}-\epsilon_k}+d_k\delta_{kk'} , \quad \text{(B5)}$$

where the continuous nature of the eigenvalue spectrum has made it necessary to add a delta function with an unknown normalization constant d_k. Again using the completeness of the states $|k\rangle$, we can express the matrix element $\langle k|V|k'\sim\rangle$ in terms of the overlap matrix, and by means of the separable ansatz (2.25) and Eq. (B3) we obtain $\langle k|V|k'\sim\rangle=V_0p_{ck}\tilde{p}_{ck'}$. Thus,

$$S_{kk'}=V_0\frac{p_{ck}^*\tilde{p}_{ck'}}{\epsilon_{k'}-\epsilon_k}+d_k\delta_{kk'} . \quad \text{(B6)}$$

Inserting this expression back into Eq. (B3) and using the density of states $\mathscr{D}(\epsilon)$ to convert the sum over k to an energy integral, we obtain

$$\tilde{p}_{ck}=V_0\tilde{p}_{ck}\int\frac{A(\epsilon)}{\epsilon_k-\epsilon}d\epsilon+d_kp_{ck} . \quad \text{(B7)}$$

We have here also used the definition, Eq. (2.32), of the TDOS in the absence of the core hole, $A(\epsilon)$. Thus, it only remains to determine the normalization d_k, which we obtain from the orthonormality of the states $|k\sim\rangle$, i.e.,

$$\delta_{kk'}=\langle k\sim|k'\sim\rangle=\sum_i S_{ik}^*S_{ik'} . \quad \text{(B8)}$$

Inserting the expression (B6) for the overlap matrix into this normalization condition leads to

$$\delta_{kk'}= V_0^2 \tilde{p}^*_{ck} \int \frac{A(\epsilon)\,d\epsilon}{(\epsilon_k-\epsilon)(\epsilon_{k'}-\epsilon)} \tilde{p}_{ck'} + V_0 d_k^* \frac{p^*_{ck}\tilde{P}_{ck'}}{\epsilon_{k'}-\epsilon_k} + V_0 d_{k'} \frac{p_{ck'}\tilde{p}^*_{ck}}{\epsilon_k-\epsilon_{k'}} + |d_k|^2 \delta_{kk'} . \tag{B9}$$

The integral on the first line of this expression obviously becomes singular when ϵ_k equals $\epsilon_{k'}$ and we can here use the well-known mathematical identity

$$\int \frac{A(\epsilon)\,d\epsilon}{(\epsilon_k-\epsilon)(\epsilon_{k'}-\epsilon)} = \pi^2 A(\epsilon_k)\delta(\epsilon_k-\epsilon_{k'}) + \frac{1}{\epsilon_{k'}-\epsilon_k}\left[\int \frac{A(\epsilon)\,d\epsilon}{\epsilon_k-\epsilon} - \int \frac{A(\epsilon)\,d\epsilon}{\epsilon_{k'}-\epsilon}\right] . \tag{B10}$$

The last two terms of this identity give rise to two terms which cancel the second and the third terms on the right-hand side of Eq. (B9), and by means of the density of states factor $\mathcal{D}(\epsilon)$, the energy-delta function can be converted to a delta function in k and k'; $\delta(\epsilon_k-\epsilon_{k'})=\mathcal{D}(\epsilon_k)\delta_{kk'}$. Finally, introducing also the definition (2.31) of the TDOS in the presence of the core hole, $\tilde{A}(\epsilon)$, Eq. (B9) becomes

$$1 = V_0^2 \pi^2 \tilde{A}(\epsilon_k) A(\epsilon_k) + |d_k|^2 , \tag{B11}$$

which determines the normalization d_k to within a phase factor of no relevance to the final result for $\tilde{A}(\epsilon)$. The phase factor can, e.g., be chosen as $\exp(i\delta_k)$ where δ_k is the phase shift. This choice can be seen to correspond to ordinary scattering theory or T-matrix theory, whereas a choice of unity corresponds to scattering theory based on the reaction matrix.[61] Preferring real quantities, we made the latter choice. Inserting the result given by Eq. (B11) into Eq. (B7), we obtain $\tilde{p}_{ck}$ and thus $\tilde{A}(\epsilon)$ from the definition (2.31). This leads to Eq. (2.36) of the main text.

Equation (B11) allows us to write

$$\cos\delta_k = d_k , \tag{B12}$$

$$\sin\delta_k = -\pi V_0 [A(\epsilon_k)\tilde{A}(\epsilon_k)]^{1/2} , \tag{B13}$$

in terms of an angle δ_k, which obviously is positive for attractive potentials ($V_0<0$) and tends linearly to zero with the potential. It is not difficult to see that δ_k defined in this way corresponds to the usual definition of a scattering phase shift.[61] The Eq. (2.36) then also gives the convenient relation

$$\tan\delta_k = -\pi V_0 A(\epsilon_k)\left[1 - V_0 \int \frac{A(\epsilon)\,d\epsilon}{\epsilon_k-\epsilon}\right]^{-1} . \tag{B14}$$

Finally, from the Eqs. (B6), (B7), (B12), and (B14) we arrive at the following expression for the overlap matrix S

$$S_{kk'} = \frac{1}{\pi}\frac{p^*_{ck}p_{ck'}}{\epsilon_k-\epsilon_{k'}}\frac{\sin\delta_{k'}}{A(\epsilon_{k'})} + \cos\delta_{k'}\delta_{kk'} . \tag{B15}$$

APPENDIX C

We will here use a method due to Muskhelishvili[60] to solve the integral equation (6.11). The Cauchy integrals

$$\Gamma(z) = \int_{-\infty}^{\epsilon_F} \frac{d\epsilon'}{2\pi i}\frac{\gamma(\epsilon')}{\epsilon'-z} - \rho\int_{\epsilon_F}^{\infty}\frac{d\epsilon'}{2\pi i}\frac{A(\epsilon')}{\epsilon'-z} \tag{C1}$$

define two analytic functions, one in the upper half of the complex z plane and one in the lower half. Denoting the limiting values of these functions on the real axis by $+$ and $-$ and concentrating on the part of the axis to the left of ϵ_F, we obtain

$$\Gamma^{\pm}(\epsilon) = \int_{-\infty}^{\epsilon_F} \frac{d\epsilon'}{2\pi i}\frac{\gamma(\epsilon')}{\epsilon'-\epsilon} - \rho\int_{\epsilon_F}^{\infty}\frac{d\epsilon'}{2\pi i}\frac{A(\epsilon')}{\epsilon'-\epsilon} \pm \frac{1}{2}\gamma(\epsilon) , \quad \epsilon<\epsilon_F . \tag{C2}$$

The integral equation (6.11) can then be written as

$$\Gamma^+(\epsilon) - \Gamma^-(\epsilon) + i\tan\delta(\epsilon)[\Gamma^+(\epsilon)+\Gamma^-(\epsilon)] = 0 \tag{C3}$$

or

$$\Gamma^+(\epsilon)e^{i\delta(\epsilon)} = \Gamma^-(\epsilon)e^{-i\delta(\epsilon)} . \tag{C4}$$

This relation immediately suggests the introduction of the function

$$\Phi(z) = \exp\left[\int_{-\infty}^{\epsilon_F}\frac{d\epsilon'}{\pi}\frac{\delta(\epsilon')}{\epsilon'-z}\right] , \tag{C5}$$

which obviously is analytic everywhere except for a branchcut along the real axis to the left of ϵ_F. This implies

$$\frac{\Phi^+(\epsilon)}{\Phi^-(\epsilon)} = e^{2i\delta(\epsilon)}, \quad \epsilon<\epsilon_F \tag{C6}$$

and, therefore, the function $\Gamma(z)\Phi(z)$ is continuous across the real axis to the left of ϵ_F. To the right of ϵ_F, however, it has a discontinuity across the axis of magnitude $-\rho A(\epsilon)\Phi(\epsilon)$. Thus, defining also the function

$$\Pi(z)=-\rho\int_{\epsilon_F}^{\infty}\frac{d\epsilon'}{2\pi i}\frac{A(\epsilon')\Phi(\epsilon')}{\epsilon'-z}\ , \tag{C7}$$

which obviously is analytic everwhere except at the discontinuity across the real axis to the right of ϵ_F, we see that the function $\Gamma(z)\Phi(z)-\Pi(z)$ is analytic everywhere. Since this function by virtue of Eqs. (C1), (C5), and (C7) tends to zero at infinity, it must vanish everywhere and we have

$$\Gamma(z)=\frac{\Pi(z)}{\Phi(z)}\ . \tag{C8}$$

Below the Fermi level ($\epsilon<\epsilon_F$) we can now obtain the solution $\gamma(\epsilon)$ to the integral equation (6.11) from Eqs. (C2), (C8), and (C5). We have

$$\gamma(\epsilon)=\Gamma^{+}(\epsilon)-\Gamma^{-}(\epsilon)=\Pi(\epsilon)\left[\frac{1}{\Phi^{+}(\epsilon)}-\frac{1}{\Phi^{-}(\epsilon)}\right]$$

$$=\frac{\Pi(\epsilon)}{\Phi(\epsilon)}(e^{-i\delta(\epsilon)}-e^{i\delta(\epsilon)})$$

$$=-2i\frac{\Pi(\epsilon)}{\Phi(\epsilon)}\sin\delta(\epsilon)\ , \tag{C9}$$

where the unsuperscripted functions on the real axis are obtained by replacing z by ϵ in the corresponding functions of a complex argument. Notice that the function $\Pi(z)$ is continuous across the real axis below ϵ_F. The function $\Pi(\epsilon)$ turns out to vary rather slowly over the occupied band, whereas both $\Phi(\epsilon)$ and $\sin\delta(\epsilon)$ can have appreciable structure. For instance, for strong core-hole potentials, the phase shift exhibits a resonant behavior towards the bottom of the band as does the TDOS in the presence of a core hole. In an attempt to make the structure of $\gamma(\epsilon)$ more apparent by eliminating the factor $\sin\delta(\epsilon)$ from Eq. (C9), we rewrite Eq. (B14) of Appendix B,

$$A(\epsilon)+\frac{1}{\pi}\tan\delta(\epsilon)\int\frac{A(\epsilon')\,d\epsilon'}{\epsilon'-\epsilon}=-\frac{1}{V_0\pi}\tan\delta(\epsilon)\ . \tag{C10}$$

Clearly this can be viewed as an integral equation that determines $A(\epsilon)$ if the phase shift $\delta(\epsilon)$ is known for all energies. This equation is exactly of the same type as Eq. (6.11) and we leave it to the interested reader to solve Eq. (C10) using the procedure demonstrated above in the case of Eq. (6.11). The result is

$$A(\epsilon)=-\frac{1}{V_0\pi}\sin\delta(\epsilon)\exp\left[\frac{1}{\pi}\int\frac{\delta(\epsilon')\,d\epsilon'}{\epsilon-\epsilon'}\right]\ . \tag{C11}$$

The expression

$$\eta(\epsilon)=\exp\left[\frac{1}{\pi}\int_{\epsilon_F}^{\infty}\frac{\delta(\epsilon')}{\epsilon-\epsilon'}\,d\epsilon'\right]\ , \tag{6.13}$$

defining the function $\eta(\epsilon)$, has a denominator which varies slowly for energies sufficiently below the Fermi level ϵ_F and we expect a slow variation over most of the occupied band also for $\eta(\epsilon)$. Using Eq. (C11) the function $\gamma(\epsilon)$ can now be expressed in terms of $\eta(\epsilon)$,

$$\gamma(\epsilon)=2\pi i V_0\Pi(\epsilon)\frac{A(\epsilon)}{\eta(\epsilon)}\ . \tag{C12}$$

Also the function $\Pi(\epsilon)$ can be expressed in terms of $\eta(\epsilon)$ to give

$$\Pi(\epsilon)=\frac{1}{2\pi i V_0}\frac{\rho}{\pi}\int_{\epsilon_F}^{\infty}\frac{\eta(\epsilon')\sin\delta(\epsilon')}{\epsilon'-\epsilon}\,d\epsilon'\ . \tag{C13}$$

The last two equations give Eq. (6.12) of the main text.

[1]A. J. McAlister, Phys. Rev. 186, 595 (1969).
[2]L. Smrčka, Czech. J. Phys. B 21, 683 (1971).
[3]T. McMullen, J. Phys. C 3, 2178 (1970).
[4]R. P. Gupta and A. J. Freeman, Phys. Rev. Lett. 36, 1194 (1976); Phys. Lett. 59A, 223 (1976).
[5]P. H. Citrin, G. K. Wertheim, and M. Schlüter, Phys. Rev. B 20, 3067 (1979).
[6]U. von Barth and G. Grossmann (unpublished).
[7]Lithium is an exception among the simple metals due to the large effects of incomplete relaxation of phonons (Ref. 8).
[8]C.-O. Almbladh, Phys. Rev. B 16, 4343 (1977).
[9]U. von Barth and G. Grossmann, Solid State Commun. 32, 645 (1979).
[10]M. Ya. Amusia, in *Atomic Physics 5, Proceedings of the Fifth International Conference on Atomic Physics,*

edited by R. Marrus, M. Prior, and H. Shugart (Plenum, New York, 1977), pp. 537–565.

[11]Further clues towards the final-state rule were provided by the analytical structure of the theory by Nozières and De Dominicis (Ref. 12) and by the numerical evaluations of this theory presented by Grebennikov *et al.* (Ref. 13).

[12]P. Nozières and C. T. De Dominicis, Phys. Rev. 178, 1097 (1969).

[13]V. I. Grebennikov, Yu. A. Babanov, and O. B. Sokolov, Phys. Status. Solidi. B 80, 73 (1977).

[14]U. von Barth and G. Grossmann, *Proceedings of the Vth International Conference on Vacuum Ultraviolet Radiation Physics, Montepellier, France, 1977,* edited by M. C. Castex, M. Pouey, and N. Pouey (Centre National de la Recherche Scientifique, Mendon, France, 1977) Vol II, p. 18; see also, L. Hedin, J. Phys. (Paris) 39, C4–103 (1978).

[15]U. von Barth and G. Grossmann, Phys. Scr. 21, 580 (1980).

[16]T. A. Callcott, E. T. Arakawa, and D. L. Ederer, Phys. Rev. B 18, 6622 (1978).

[17]S. E. G. Slusky, S. E. Schnatterly, and P. C. Gibbons, Phys. Rev. B 20, 379 (1979).

[18]J. J. Ritsko, S. E. Schnatterly, and P. C. Gibbons, Phys. Rev. B 10, 5017 (1974).

[19]S. E. G. Slusky, P. C. Gibbons, S. E. Schnatterly, and J. R. Fields, Phys. Rev. Lett. 36, 326 (1976).

[20]L. Ley, F. R. McFeely, S. P. Kowalczyk, J. G. Jenkin, and D. A. Shirley, Phys. Rev. B 11, 600 (1975).

[21]H. Neddermeyer, Phys. Rev. B 13, 2411 (1976).

[22]A solution to the ND problem for a square-well potential in a free-electron gas has also been obtained by Mahan (Ref. 23) using a time-dependent determinantal approach due to Combescot and Nozières (Ref. 24). Although the final-state rule is apparent from this work, the numerical resolution was not good enough to fully assess the accuracy of the rule.

[23]G. D. Mahan, Phys. Rev. B 21, 1421 (1980).

[24]M. Combescot and P. Nozières, J. Phys. (Paris) 32, 913 (1971).

[25]J. D. Dow, J. Phys. F 5, 1113 (1975).

[26]F. K. Allotey, Phys. Rev. 157, 467 (1967); Solid State Commun. 9, 91 (1971).

[27]G. W. Bryant and G. D. Mahan, Phys. Rev. B 17, 1744 (1978).

[28]J. Friedel, Comments Solid State Phys. 2, 21 (1969).

[29]C. A. Swarts, J. D. Dow, and C. P. Flynn, Phys. Rev. Lett. 43, 158 (1980).

[30]J. Friedel, Philos. Mag. 43, 153 (1952); 43, 1115 (1952).

[31]A. Kotani and Y. Toyozawa, J. Phys. Soc. Jpn. 35, 1073 (1973); 35, 1082 (1973); 37, 912 (1974).

[32]G. D. Mahan, Phys. Rev. 163, 612 (1967).

[33]P. W. Anderson, Phys. Rev. Lett. 18, 1049 (1967).

[34]C.-O. Almbladh and L. Hedin, *Beyond the one-electron model; Many-electron effects in atoms, molecules and solids,* in *Handbook of Synchrotron Radiation,* edited by E. E. Koch (North-Holland, Amsterdam, 1982) Vol. I.

[35]P. Minnhagen, J. Phys. F 7, 2441 (1977). The importance of dynamical screening is stressed in this paper but the small difference between including or not including (ND) this effect is not essential on the scale of the present discussion.

[36]C.-O. Almbladh, in Extended Abstracts of the VIth International Conference on Vacuum Ultraviolet Radiation Physics, University of Virginia, 1980 (unpublished), Vol. I, p. 33.

[37]P. H. Citrin, G. K. Wertheim, and Y. Baer, Phys. Rev. B 16, 4256 (1977).

[38]G. K. Wertheim and P. H. Citrin, in *Photoemission in Solids I,* Vol. 26 of *Topics in Applied Physics,* edited by M. Cardona and L. Ley (Springer, Berlin, 1978), pp. 197–236.

[39]P. Steiner, H. Höchst, and S. Hüfner, in *Photoemission in Solids II,* Vol. 27 of *Topics in Applied Physics,* edited by L. Ley and M. Cardona (Springer, Berlin, 1979), pp. 349–372.

[40]J. D. Dow and C. P. Flynn, J. Phys. C 13, 1341 (1980).

[41]M. A. Bowen and J. D. Dow, Phys. Rev. B 22, 220 (1980).

[42]By varying the parameters of model systems beyond the physically accessible regime, it is, however, possible to destroy this equivalence as shown by Bowen and Dow (Ref. 41).

[43]D. C. Langreth, Phys. Rev. 182, 973 (1969).

[44]In the ND model we introduce a statically screened potential V into the free-electron gas. From perturbation theory we obtain the second-order contribution Δ_2^{ND} to the "relaxation" shift Δ_r of ND theory,

$$\Delta_2^{\mathrm{ND}}=-\tfrac{1}{2}\int \chi_0(\underline{q})\,|\,V(\underline{q})\,|^2 d^3q/(2\pi)^3 .$$

Here, $\chi_0(\underline{q})$ is the static wave-vector-dependent density-response function of the free-electron gas (the Lindhart function). In a more elaborate theory we introduce a bare core-hole potential, $w(\underline{r})$, into the interacting electron gas. There is then a linear term which is, however, cancelled by a term describing the core-hole interacting with the positive background. The second-order contribution, Δ_2, to the relaxation shift is given by

$$\Delta_2=-\tfrac{1}{2}\int \chi(\underline{q})\,|\,w(\underline{q})\,|^2 d^3q/(2\pi)^3 ,$$

where $\chi(\underline{q})$ is the static density-response function of the interacting electron gas and $w(\underline{q})$ is the Fourier transform of $w(\underline{r})$. In linear Hartree theory we have $V=w/\epsilon$ and $\chi=\chi_0/\epsilon$ giving

$$\Delta_2=-\tfrac{1}{2}\int \chi_0(\underline{q})\,|\,V(\underline{q})\,|^2\epsilon(\underline{q})\,d^3q/(2\pi)^3 ,$$

where $\epsilon(\underline{q})$ is the static dielectric function. Thus, the ND result Δ_2^{ND} is clearly different from the correct result Δ_2. This is a deficiency of the ND theory which need not concern us here, since we are only interested

in line shapes and not in threshold positions.

[45]J. S. R. Chisholm, J. Math. Phys. 4, 12, 1506 (1963).

[46]This is borne out in that the fitting procedure results in parameters Ω_0 and Ω which are very close to $\epsilon_F - \epsilon_B$, where ϵ_B is the bottom of the band.

[47]B. Vinter, Phys. Rev. B 17, 2429 (1978).

[48]L. Hedin, in *X-ray Spectroscopy,* edited by L. V. Azaroff (McGraw-Hill, New York, 1974), p. 226.

[49]Owing to an unphysical choice of potential in some cases discussed by Dow and Flynn (Ref. 40) the states $|N,s\sim\rangle$ do not form a complete set and, consequently, the resulting spectrum does not fulfill the sum rule, Eq. (3.7).

[50]Note that $V_{kk'}=V_0 p^*_{ck} p_{ck'}$, see Eq. (2.25).

[51]P. Minnhagen, Phys. Lett. 56A, 327 (1976).

[52]P. Nozières, *Theory of Interacting Fermi Systems* (Benjamin, New York, 1964).

[53]The analysis in Sec. VI suggests that the limit

$$\lim_{N\to\infty} C_1 \,|\langle N\sim|N\rangle|^{-2} J_1^{(N)}(\omega)$$

is a reasonable choice for the spectrum $J_1(\omega)$, provided C_1 is a suitably chosen normalization constant independent of N. A similar definition can be chosen for the spectrum $J_2(\omega)$, etc.

[54]C.-O. Almbladh and U. von Barth, Phys. Rev. B 13, 3307 (1976).

[55]The energy variation of $C(\omega)$ for strong core-hole potentials is actually a spurious effect due to the fact that, for large threshold exponents α_0, the enhancement factor $[\epsilon_F/(\epsilon_F-\omega)]^{\alpha_0}$ has a non-negligible energy variation also away from threshold. As shown in Sec. VI this factor is more accurately given by an expression of the form $1+a[\epsilon_F/(\epsilon_F-\omega)]^{\alpha_0}$.

[56]Swarts *et al.* (Ref. 29) were asked by the referee to analyze their data according to Eq. (4.3).

[57]C. Kunz, R. Haensel, G. Keitel, P. Schreiber, and B. Sonntag, in *Electronic Density of States,* U. S. Natl. Bur. Stand. Spec. Publ. No. 323, edited by L. H. Bennett (U. S. GPO, Washington, D. C., 1971), p. 275.

[58]Notice that the spectrum d_2 is negative below the bottom of the band. This is no numerical artifact but is due to the fact that the spectrum obtained from the transient Green's function only, i.e., by setting $\tilde{g}(t)=1$ in Eq. (2.27), is unphysical. Only the product $\tilde{g}(t)\tilde{G}(t;t)$ [Eq. (2.21)] has physical relevance.

[59]D. C. Langreth, Phys. Rev. B 1, 471 (1970).

[60]N. I. Muskhelishvili, *Singular Integral Equations* (Noordhoft, Groningen, 1953).

[61]M. L. Goldberger and K. M. Watson, *Collision Theory* (Wiley, New York, 1964).